eNeuro

Research Article: New Research | Sensory and Motor Systems

Transcriptomic Signatures of Postnatal and Adult Intrinsically Photosensitive Ganglion Cells

https://doi.org/10.1523/ENEURO.0022-19.2019

Cite as: eNeuro 2019; 10.1523/ENEURO.0022-19.2019

Received: 17 January 2019
Revised: 19 July 2019
Accepted: 23 July 2019

Manuscript title: Transcriptomic Signatures of Postnatal and Adult Intrinsically Photosensitive Ganglion Cells

Authors:

Daniel Berg[1,2], Katherine Kartheiser[2], Megan Leyrer[2], Alexandra Saali[2], David Berson[2]

1. Molecular biology, Cellular biology, and Biochemistry (MCB) Program

2. Department of Neuroscience

Brown University, Providence, RI 02912

Correspondence to: David Berson (david_berson@brown.edu)

Abstract

Intrinsically photosensitive retinal ganglion cells (ipRGCs) are rare mammalian photoreceptors essential for non-image-forming vision functions, such as circadian photoentrainment and the pupillary light reflex. They comprise multiple subtypes distinguishable by morphology, physiology, projections, and levels of expression of melanopsin (Opn4), their photopigment. The molecular programs that distinguish ipRGCs from other ganglion cells and ipRGC subtypes from one another remain elusive. Here, we present comprehensive gene expression profiles of early postnatal and adult mouse ipRGCs purified from two lines of reporter mice that mark different sets of ipRGC subtypes. We find dozens of novel genes highly enriched in ipRGCs. We reveal that *Rasgrp1* and *Tbx20* are selectively expressed in subsets of ipRGCs, though these molecularly defined groups imperfectly match established ipRGC subtypes. We demonstrate that the ipRGCs regulating circadian photoentrainment are diverse at the molecular level. Our findings reveal unexpected complexity in gene expression patterns across mammalian ipRGC subtypes.

Significance statement: A comprehensive transcriptomic analysis has identified dozens of genes differentially expressed in intrinsically photosensitive retinal ganglion cells, including some linked to signaling, gene regulation, and melanopsin phototransduction.

Introduction

Many unique attributes distinguish intrinsically photosensitive retinal ganglion cells (ipRGCs) from conventional RGCs. Only ipRGCs express the blue-light sensitive photopigment melanopsin (OPN4), which renders them autonomously light-sensitive. They violate the usual stratification rule in which ON-type RGCs deploy their dendrites only in the inner (proximal) half of the inner plexiform layer; their inputs from ON bipolar cells are atypical (Dumitrescu et al., 2009; Hoshi et al., 2009; Kim et al., 2010). Whereas most RGCs direct their entire output through the optic nerve, some ipRGCs modulate intraretinal processing, through amacrine cells (Reifler et al., 2015; Sabbah et al., 2017; Zhang et al., 2008; Xue et al., 2011) and spontaneous retinal waves during the early postnatal period (Renna et al., 2011). Functionally, ipRGCs are unique among RGCs in their ability to encode overall light intensity for extended periods (Wong, 2012). This tonic luminance signal is transmitted to specific brain targets for a variety of functions including photoentrainment of circadian rhythms and light evoked pupillary constriction. Additionally, ipRGCs appear more resistant than RGCs overall to various insults, including optic nerve injury, glutamate-induced excitotoxicity, and glaucoma (Cui et al., 2015).

The ipRGCs consist of at least six anatomically distinct retinal subtypes, termed M1-M6 (Figure 1A). These differ in their level of melanopsin expression, visual response properties, dendritic stratification, axonal projections, and contributions to light-modulated behavioral responses (Schmidt et al., 2011). The suprachiasmatic nucleus (SCN) receives projections primarily from M1 ipRGCs, but also a minor input from the M2 subtype (Viney et al., 2007; Baver et al., 2008). The ipRGCs project to distinct regions of the midbrain, with M1 and M2 ipRGC

axons arriving to the shell and core of the olivary pretectal nucleus (OPN), respectively (Prichard et al., 2002; Baver et al., 2008; Güler et al., 2008). The OPN also receives significant input from the recently described M6 ipRGCs (Quattrochi et al., 2019). M2-M4 ipRGCs send projections to image-forming brain regions and mediate coarse pattern vision, while spectrally opponent M5 cells contribute to color vision (Ecker et al., 2010; Estevez et al., 2012; Stabio et al., 2018; Sonoda et al., 2018).

The distinctive structural and functional properties of ipRGCs must ultimately be traceable to different patterns of gene expression that have remained elusive. The melanopsin phototransduction cascade is a major defining feature of ipRGCs and the basic molecular framework has been identified (see Hughes et al., 2012 for review). However, the precise phototransduction mechanisms across the ipRGC subtypes have only recently become characterized (Sonoda et al., 2018; Jiang et al., 2018). M1 ipRGCs have been further subdivided based on their expression of the transcription factor Pou4f2 (Brn3b) (Chen et al., 2011; Jain et al., 2012). Ablation of Brn3b-positive ipRGCs severely impairs the pupillary light reflex, but leaves circadian photoentrainment intact (Chen et al., 2011). Further, Brn3b-positive M1 ipRGCs provide inputs to diverse brain regions including the thalamus, midbrain, and hypothalamus (Li and Schmidt, 2018). Additionally, the transcription factor Tbr2 is selectively expressed in adult ipRGCs (Mao et al., 2014; Sweeney et al., 2014). Further molecular diversity is expected among ipRGCs, both within and between established ipRGC subtypes.

Previous attempts to develop a “molecular parts list” for ipRGCs through gene-expression profiling of adult ipRGCs have been limited by the extreme heterogeneity of retinal tissue and the fragility of mature retinal neurons (Lobo et al., 2006; Heiman et al., 2008; Sanes and Masland, 2015). Prior efforts using either anti-melanopsin immuno-panning or fluorescence-activated cell sorting (FACS) of genetically-labeled fluorescent ipRGCs have been limited by low yield and inclusion of contaminating cell populations such as rods (Hartwick et al., 2007; Peirson et al., 2007; Siegert et al., 2012).

Here we conducted a thorough unbiased transcriptomic analysis of ipRGCs by purifying GFP-tagged ipRGCs through a combination of FACS and immunoaffinity and comparing with the transcriptional profile of GFP-negative RGCs. We did this in two different mouse lines, marking partially overlapping subsets of ipRGCs. The specificity and purity of these ipRGC samples is validated by their substantial enrichment for transcripts of genes known to be selectively expressed in ipRGCs and very low expression levels of genes linked to potentially contaminating cell types. We identified more than 75 new gene candidates expressed much more highly in adult ipRGCs than in other RGCs. We validate two of the new molecular markers at the protein level: Rasgrp1, which is a Ras guanine nucleotide exchange factor (Ras GEF); and Tbx20, a T-box transcription factor. We relate these novel markers to established ipRGC subtypes and patterns of central projection.

Materials and Methods

Animals

All experiments were conducted in accordance with NIH guidelines under protocols approved by the Brown University (Providence, RI) Animal Care and Use Committee. Both male and female adult mice (P30 to P90) were used unless otherwise stated. *Opn4*$^{cre/cre}$ mice were crossed with floxed-stop reporter mice: "*Z/EG*" (*Jax#003920*); the offspring express GFP in *cre*-expressing cells (M1-M6), as described by Ecker et al., 2010. *Opn4-GFP(ND100Gsat)* is a BAC transgenic mouse generated by the GENSAT project at Rockefeller University. The Rasgrp1-KO (Rasgrp1^{tm1Jstn}, Dower et al., 2000) was initially provided generously by Robert Barrington, U. of Alabama for initial testing. The *Cdh3-GFP* reporter is a BAC transgenic originally generated by the Gensat project (MMRRC, BK102Gsat/MMNC) useful for identifying M6 ipRGCs (Quattrochi et al., 2019). This mouse line was backcrossed with C57BL/6J background for >10 generations. *Cdh3-GFP* mice were three weeks old or younger unless otherwise stated.

105 *Retinal dissociation*

106 Mice from either postnatal day 5 (+/- 1day) or young adult (P30 +/- 3 days) mice were
107 euthanized by inhalation of CO_2. Retinal tissue was dissected free into room temperature
108 Hibernate-A medium (BrainBits). At least three biological replicates were produced for each
109 dataset: three replicates for immature Gensat *Opn4-GFP* mice (postnatal day 4-6; P4-6); six for
110 adult Gensat *Opn4-GFP* mice; and four for *Opn4*$^{Cre/+}$*; Z/EG*$^{+/-}$). We were able to regularly isolate
111 more than 10,000 GFP+ ipRGCs from nine postnatal day 5 (P5) transgenic reporter mice. In
112 contrast, each adult replicate required 15-20 mice to obtain sufficient cells for the transcriptional
113 analysis due the relative fragility of adult retinal ganglion cells.

114 Fresh retinas were enzymatically dissociated in a medium containing 10 mL of
115 Hibernate-A minus Calcium (Brainbits), 20U/mL papain (Worthington), 0.25% Glutamax (Gibco),
116 1mM L-Cysteine, 0.004% DNase, and titrated to 7.4 pH with NaOH. The dissociation medium
117 was activated for 30 minutes at 37°C before retinal immersion. Retinas were incubated in it for
118 45 minutes, with gentle shaking every 5-10 minutes, then centrifuged for 3 minutes at 200 rcf
119 and washed with 1 mL of trituration medium containing Hibernate-A and 10% Fetal Calf Serum
120 (FCS). Retinas were gently triturated 10-15 times with a P1000 tip and an additional 4 mL of
121 trituration buffer was added to each tube. The retina cell suspension was centrifuged for 11
122 minutes at 1000 rcf. The pellet was washed and resuspended with 1mL of HABG buffer
123 containing Hibernate-A, 0.25% BSA, 1% B27 (Gibco), and 0.25% Glutamax (Gibco).
124
125 *RGC Pre-Enrichment*

126 As a first step to purifying ipRGCs from dissociated retinal cells, we selected for ganglion
127 cells by immunoaffinity for the cell-surface protein Thy-1 (Barres et al., 1988; Cahoy et al.,
128 2008). We adapted classic immunopanning procedures to a magnetic-activated cell-sorting
129 approach (MACS, Miltenyi Biotec). We incubated 1 mL of dissociated retinal cell suspension
130 with 100 µl Thy1(CD90.2)-conjugated magnetic nanoparticles (Miltenyi) for 15 minutes at room

temperature. The cell suspension was then passed through a Pre-separation filter and MS column (Miltenyi), which retained cells bound to Thy1-magnetic beads within the column magnetic field. After rinsing with HABG media, the remaining cells were flushed with 1 mL HABG media. In preparation for FACS, 2ul/mL of the DNA intercalating dye 7-AAD (BD Pharmingen), was added to the solution to mark cells with compromised cell membranes.

Fluorescence-Activated Cell Sorting (FACS)

The RGC-enriched cell suspension obtained from the immunoaffinity step was passed through a FACS Aria (BD Biosciences) electrostatic sorter. Dead and dying cells were excluded based on high deep red 7-AAD fluorescence. We also excluded cellular debris, which registered as being essentially non-fluorescent, with relatively lower forward light scatter (FSC; an indication of particle size) and side light scatter (SSC; granularity) compared to RGCs.

The remaining cells were sorted using FITC gating into GFP-positive cells (presumptive ipRGCs in either reporter mouse we used; Figure 2) and GFP-negative cells (nearly all expected to be conventional RGCs; cRGCs). The goal was to compare the transcriptional profiles of these two matched samples to identify genes differentially over- or under-expressed in ipRGCs. The cRGC and ipRGC samples were treated with the same reagents, cytometer settings, centrifugation forces, and temperatures throughout the procedure. cRGCs and ipRGCs had similar SSC and FSC values.

RNA Extraction and cDNA Preparation

RNA-processing was done in an enclosed RNase-free environment to limit degradation of RNA throughout the extraction process. FACS-acquired cells were sorted directly into Qiagen RLT buffer with 10 uL/mL of β-mercaptoethanol for immediate lysis. While sorting, the lysis solution was kept at 4°C and periodically mixed. After sorting, we extracted the RNA from the lysed cells using the RNeasy Micro Kit and RNeasy Minelute columns (Qiagen). The enriched

RNA was treated on-column with RNase-free DNase I (RNeasy Micro Kit) to remove any residual genomic DNA from the sample. For RNA elution, 12 µl of RNase-free water was added directly to the center of the spin column membrane and centrifuged at >8000 rcf for 1 minute. 5 µl of eluted RNA solution was retained for Nugen Ovation cDNA amplification (Caretti et al., 2008; Clément-Ziza et al., 2009; Morse et al., 2010; Tariq et al., 2011). Additionally, integrity of eluted RNA was assessed using PicoChip RIN analysis and RNA amount using the Qubit RNA assay. Initially, we proceeded immediately with cDNA processing after RNA extraction. However, freezing at -80°C did not alter RNA integrity since the frozen RNA samples still received RIN score of 9.0 or greater. Therefore, most of the cDNA libraries were prepared after storage of extracted RNA at -80°C.

RNA-seq library preparation and sequencing

Before preparing sequencing libraries, we first sheared cDNA to the appropriate size, (200-300bp median) using the Covaris system. Each sample was subsequently processed using Illumina Truseq kit using a unique barcode adapter to allow for multiplexing multiple samples. Excess adapter sequences were removed using Ampure bead isolation, which removes all DNA fragments less than 200bp. The library fragment size distribution was tested using High Sensitivity Bioanalyzer) and qPCR analysis using primers that match the library adapters (Quail et al., 2008) (Figure 3D). Finally, 50 bp single-end sequencing was completed using HiSeq 2000 (approximately 200 million reads divided among sequencing samples). Initially, we processed 8 samples per lane with multiplexed sequencing. We later ran many of the sequencing libraries again with less multiplexing, providing increased sequencing depth. The corresponding technical replicates were merged together for differential expression analysis. The final read counts of each sample are shown in Figure 3D.

Differential gene and transcript expression analysis

For the tens of millions of reads generated by sequencing we first removed adapter sequences and low-quality reads using fastx_clipper and fastq_quality_filter, respectively. Second, using tophat2 we aligned reads to the mm9 mouse reference genome. Third, the aligned reads were converted to SAM format for htseq-count, which counted the number of reads that aligned to an annotated gene. Finally, we used the EdgeR package to perform statistical analysis on the generated count table to identify quantitative differences in expression levels between the two experimental samples (Anders and Huber, 2010; Trapnell et al., 2012; Anders et al., 2013). EdgeR compares and retains the relationship between all pairs of experimental samples when calculating differential expression likelihood (Anders et al., 2013). Our analysis filtered out genes with very low counts, less than 1 count per million (cpm), in more than half of the samples used in the differential expression analysis.

Identification of differentially expressed genes

To identify the set of differentially expressed genes (DEGs) in the ipRGC populations, we used the following strict criteria. First, we identified genes with low false discovery rate (FDR < 0.05) and high fold-change (greater than 2-fold) suggesting differential expression between ipRGCs and generic RGCs. Second, we considered whether the differentially gene expression was corroborated across both reporters (*Opn4::GFP* labeling M1-M3 cells and the *Opn4::Cre/GFP* system that labels M1-M6 ipRGCs) and both ages (postnatal day 5 (+/- 1day) or young adult (P30 +/- 3 days). Third, we identified whether the DEGs have nearly absent gene expression in cRGC samples to distinguish potential for selective gene expression in ipRGCs. This was distinguished both at the level of count-values and manual inspection of aligned raw reads using the Integrated Genome Viewer (IGV) (Thorvaldsdóttir and Robinson, 2013). Using IGV, we verified that the reads align with reference gene model for full-length coverage across multiple ipRGC replicates and that there were absent or partial reads aligned across the generic RGC replicates.

Determining differentially *repressed* genes in adult ipRGCs was confounded by the high amount of contaminants in generic RGC populations. We could not decipher whether a gene with relatively low expression in ipRGCs was the result of non-RGC populations contaminating the generic RGC control population. In contrast, the P5 generic RGC samples from the *Opn4-GFP* reporter were determined to have greatly reduced levels of contamination and similar levels of RGC marker expression (Figure 5). This made it possible to identify genes more weakly expressed in ipRGCs than in generic RGCs in early postnatal development (Figure 7).

Accession of RNA-Seq data

Deposited in NCBI GEO with accession number GSE118780. To review GEO accession, Go to https://www.ncbi.nlm.nih.gov/geo/query/acc.cgi?acc=GSE118780

Enter token knstamamblqhpuh into the box (please keep access code confidential)

Retina Tissue Preparations and Solutions

Mice were euthanized by inhalation of CO_2. Prior to removing the eye, the dorsal margin of the cornea was marked with a cautery and this was used to guide the placement of a large relieving cut in the dorsal retina as a subsequent guide to retinal orientation. Eyes were removed immediately after death and placed in Hibernate-A solution preheated to 37 °C. To keep track of retinal orientation, the right and left eye were identified and processed separately.

Immunohistochemistry

The following primary antibodies were used for our immunofluorescence co-labeling studies: rabbit anti-melanopsin (Advanced Targeting Systems; 1:10,000), guinea pig anti-RBPMS (PhosphoSolutions 1832-RBPMS), rabbit anti-green fluorescent protein (GFP; Invitrogen); Goat anti-Brn3b antibody (Santa Cruz #sc-6026); mouse anti-Rasgrp1 (Santa Cruz sc-8430); guinea pig anti-Tbx20[1:8500] (Song et al., 2006). Secondary antibodies consisted of

Alexa Fluor 350, 488, 594 or 647 donkey anti-goat, Alexa Fluor 594 donkey anti-rabbit and Alexa Fluor 594 goat anti-guinea pig (Invitrogen or Jackson Immunoresearch).

For immunofluorescence studies, the dissected retina was flattened onto Millipore nitrocellulose paper after making four small relieving cuts and fixed for 30 minutes at room temperature (freshly prepared 4% paraformaldehyde in 0.1M phosphate buffered saline; PBS; pH 7.4). The tissue was then washed for 15 minutes in PBS three times, then incubated in a blocking solution of 0.5% Triton-X and 5% Goat Serum in PBS for two hours at room temperature. The tissue was incubated in the primary antibodies diluted in this same blocking solution for two days at 4 °C on a shaker. The following day, the samples were washed six times for 20 minutes in 0.1% Tween-20 in PBS. The tissue was then incubated for two hours in the appropriate secondary antibodies diluted 1:1000 in the blocking solution at room temperature. The tissue was then washed six times for 10 minutes in 0.1% Tween-20 in PBS. The retinas were mounted in Aquamount, coverslipped, and sealed with fingernail polish.

For Rasgrp1 immunofluorescence studies that did not include Tbx20 immunofluorescence, an additional antigen retrieval step was included by placing fixed tissue in Tris-EDTA (pH 8.0) for 30 minutes at 80°C. The samples were then allowed to return to room temperatures (about 15-30 minutes) before they were removed from the Tris-EDTA solution and washed three times for 15 minutes in PBS.

Anti-GFP immunofluorescence using alexa fluor 488 labeled secondary antibody was included for all studies exploiting GFP labeling.

Image Acquisition

Immunofluorescent images were captured on a Zeiss Confocal (LSM 510) and Nikon Eclipse microscope (Micro Video Instruments, Inc. E614, Avon, MA) with a built in Spot Camera (Diagnostic Instruments, Inc. HRD 100-NIK Sterling Heights, MI). Confocal images were taken with a 20x objective (Plan Apochromat, WD 0.55 mm) at a resolution of 2048 pixels. To

enhance clarity, image files were pseudocolored and the brightness and contrast was adjusted using ImageJ 1.47 (National Institutes of Health, Bethesda, MD). Final images were assembled in ImageJ and Powerpoint (Microsoft Corporation, Redmond, WA).

Retrograde axon-transport labeling of ipRGCs from the suprachiasmatic nucleus

To label ipRGCs sending axon terminals to the suprachiasmatic nucleus (SCN), we used a retrograde tracing method as previously described (Estevez et al., 2012; Stabio et al., 2018). Wild type mice (4-8 weeks old) were anesthetized by inhalation of 3% isofluorane and placed in stereotaxic apparatus. A craniotomy was performed above the injection site (SCN: -0.5 AP, -5.6 DV, 1.25 ML) and a glass micropipette attached to a Picospritzer II (Parker Hannifin) was used to deliver 200 nL of retrograde tracer rhodamine latex microspheres (RetroBeads, Lumafluor). Three to five days later, the brain was removed and immediately fixed overnight at 4°C in 4% paraformaldehyde freshly prepared in 0.1M phosphate buffered saline. The following day, the brain was rinsed in 0.1M PBS and sectioned at 50um in the coronal plane. The slices were incubated in fluorescent DAPI stain to facilitate histological identification of the SCN. Fluorescence imaging allowed us to visualize the injection site (rhodamine channel) in relation to the SCN, discernable from UV DAPI fluorescence. For this, we used a SPOT RT Slider digital microscope camera mounted to a Nikon (Diagnostic Instruments) as described previously (Berson et al., 2010; Estevez et al., 2012). Images were assembled in Adobe Photoshop CS3. For all data presented, injections spared the underlying optic chiasm and tracts, thus avoiding nonspecific retrograde labeling of RGCs.

Results

For our transcriptomics studies, we enzymatically dissociated retinas from melanopsin-reporter mice, selected for RGCs by anti-Thy1 immunoaffinity, and sorted these into presumptive ipRGC and conventional ganglion-cell (cRGC) pools by FACS based on the

fluorescent labeling of ipRGCs (Figure 1B). We then compared gene expression in these ipRGC-enriched and cRGC-enriched cell samples to identify genes differentially expressed in ipRGCs as compared to other ganglion cells.

We used two strains of melanopsin-reporter mice for these experiments. One of these was a BAC transgenic mouse generated by the GENSAT project (here termed *Opn4-GFP*). Because the GENSAT *Opn4-GFP* reporter line has not been characterized previously, we using anti-melanopsin immunofluorescence to relate the pattern of GFP labeling to that obtained. The M1 and M2 ipRGCs subtypes (and the bistratified M3 variant) express enough melanopsin throughout their somas and dendrites to permit M1 and M2 cells to be differentiated based on their dendritic stratification in the IPL (OFF sublayer for M1 cells; ON sublayer for M2 cells; see Berson et al., 2010; Schmidt and Kofuji 2009). M3 ipRGCs, which are relatively rare, stratify in both the ON and OFF sublamina. Documenting this bistratified pattern in such material is labor intensive, so for efficiency, we simply grouped any cell with melanopsin immunopositive dendrites in the OFF IPL together and refer to this as the "M1/M3" type. To limit bias, identification and classification of ipRGCs based on Opn4-immunofluorescence was completed first and remained hidden from the analyst until labeling of other features were completed.

All *Opn4-GFP*$^{+}$ cells were Opn4-immunopositive (n=60 GFP^{+} cells across seven regions of one retina, Figure 2A). Approximately half of GFP^{+} cells were M1/M3 ipRGCs with somas in the ganglion-cell layer (52.6±6.8% of 66 GFP+ cells across seven retinal regions), 9.7±5.0% were displaced M1 cells, and the remaining 37.7±3.5 were M2 cells. Unexpectedly, many of the Opn4-immunopositive M1-M3 ipRGCs were not labeled by the reporter. Most, but not all, M1/M3 ipRGCs immunoreactive for anti-Opn4 also co-expressed GFP (63.3±4.8% of 55 M1 cells), while only 28.7±3.9% of M2 ipRGCs (88 cells) were GFP^{+}. Therefore, the coexpression of EGFP expression by the *Opn4-GFP* reporter is strongly correlated with M1-M3 ipRGCs, but only accounts for about half of the population. In its selective labeling of M1-M3 ipRGCs, this *Opn4-*

EGFP reporter resembles another BAC transgenic melanopsin reporter mouse of similar design (Schmidt et al., 2008). The selectivity presumably results from the fact that these ipRGC subtypes express the most melanopsin, and GFP expression is proportionate.

The other reporter mouse used in this study, *Opn4*$^{Cre/+}$*; Z/EG* mice (*Opn4-Cre/GFP*), has been previously demonstrated to label with EGFP all six known morphological types of ipRGCs, named M1–M6, while labeling few if any conventional RGCs (cRGCs) (Ecker et al., 2010; Estevez et al., 2012; Quattrochi et al., 2019; Stabio et al., 2018). M4-M6 cells have lower levels of melanopsin-expression than M1-M3 cells and their dendrites are not revealed by Opn4 immunostaining (Ecker et al., 2010; Quattrochi et al., 2019; Stabio et al., 2018). Nonetheless, M4 cells are recognizable among GFP+ cells in this mouse line from their large soma size, and weak melanopsin or absent anti-melanopsin immunolabeling (Estevez et al., 2012).

Opn4-immunofluorescence revealed that more than one-fourth of ipRGCs of the M1, M2 and M3 cells lacked discernable GFP-labeling in this reporter mouse (M1/M3 cells: 28%, n=81; displaced M1 cells: 27%, n=15; M2 cells: 33%, n=132; four sampled regions from one *Opn4-Cre/GFP* retina; Figure 2B,C). Among presumed M4 cells (large somas; faint Opn4-immunoreactivity) only about a quarter were GFP-positive (27% Opn4^{+};GFP$^{neg.}$, n=67 M4 cells). Other presumed M4 cells (large GFP+ somas) were Opn4-immunonegative (54%, n=67 M4 cells) (Figure 2C). GFP^{+} cells with small somas and no evident Opn4-immunoreactivity were designated as “unknown” ipRGC types (72%, n=202 unknown cells; Figure 2C) These were presumably mainly M5 and M6 cells, but this could not be confirmed from dendritic immunostaining. Additionally, we observed small cell bodies of unknown type with weakly Opn4-immunlabeling that did not extend to the dendrites (28%) (Figure 2C).

Cell composition and purity of isolated ipRGCs and conventional RGCs

The transcriptional data obtained offered broad internal evidence for the efficacy of purification of cell samples. As expected, the *Opn4* (melanopsin) gene was among the genes

much more highly expressed in ipRGCs than in cRGCs. For example, *Opn4* was enriched 40-fold in adult ipRGCs purified from *Opn4-GFP* mice, and this was highly significant, at $q<1x10^{-55}$ false discovery rate (FDR). Though *Opn4* expression was detected in cRGCs at modest levels (Figure 4A), this was expected, because some ipRGCs lack GFP expression in both melanopsin reporter lines (Opn4-GFP and Opn4-cre/GFP), and these would have been pooled with cRGCs during the FACS procedure.

Transcripts of other genes known to be expressed in ipRGCs were also enriched in the ipRGC pool relative to the cRGC pool (FDR < 0.05, significantly expressed in ipRGC samples, and absent or weakly expressed in cRGC samples). Among these genes were *Adcyap1* (pituitary adenylate-cyclase activating polypeptide; PACAP), *Tbr2*, (*Eomesodermin*), *Trpc7* and, to a lesser extent, *Trpc6* (Hannibal et al., 2004; Xue et al., 2011; Sand et al., 2012; Mao et al., 2014; Sweeney et al., 2014) (Figure 4A). Taken together, these results demonstrate that mRNA isolated from purified ipRGC samples were enriched as expected for transcripts for genes that are known to be differentially expressed in ipRGCs.

The relationship among the transcriptional profiles of ipRGC and cRGC samples across replicates are illustrated in the multidimensional scaling (MDS) plots of Fig. 4B. These show the relationship between all pairs of samples (one of ipRGCs, the other of cRGCs) based on a count-specific pairwise distance measure (Anders et al., 2013) (Figure 4B). These sample pairs were clearly separated along the first dimension, indicating pronounced differences in overall gene-expression patterns between ipRGC and cRGC samples. Samples of ipRGCs and cRGCs derived from the same retina and processed in parallel tended to be closely spaced along the second dimension, indicating greater similarity within than across replicates. This may reflect slight differences in overall genetic makeup of mice contributing to each pool, since both strains used were on a mixed genetic background, or to slight technical differences in the acquisition and processing of RNA from one run to the next.

In the purified ipRGC samples, we found little or no evidence of contamination by transcripts from other retinal cell types. For example, transcript levels were very low for rod and cone opsins, for the amacrine-specific marker ChAT, for several bipolar markers (Otx2; Vsx2; Grm6; Trpm1), and for markers of astrocytes, microglial and vascular cells (Figure 5). Several transcripts suitable for assessing potential contamination from Müller glia (*Glul, Vim)* were present at surprisingly high levels in the purified ipRGC samples, suggesting that these glial cells may contaminate the transcriptional picture to some degree.

In general, the cRGC samples were relatively less pure than the ipRGCs samples by this measure. A particularly informative transcript for assessing such contamination is that for the rhodopsin gene (*Rho*), because rods are by far the most common neuronal type in the mouse retina and express *Rho at* very high levels. Rhodopsin transcripts were significantly (150-fold) more abundant in the cRGC samples than in ipRGC samples (Figure 5), whether isolated from *Opn4-GFP* or *Opn4-Cre/GFP* adult reporter mice (FDR < 6 x 10^{-9}). Evidently, the second isolation step in which GFP+ positive cells were isolated by FACS from the purified RGC pool was a key factor in the greater purity of the ipRGC sample. Similarly, transcripts associated with bipolar cells and Müller glial cells were generally more abundant in cRGC than ipRGC samples. For example, the cRGCs had relatively high expression of the known Müller glia markers *Glul*, *Apoe*, *Aqp4*, and *Vim*, generally higher than in the ipRGC pool (Figure 5). Contamination of adult cRGC samples by other cell types may explain why most RGC markers, such as *Rbpms* and *Sncg* (Soto et al., 2008; Rodriguez et al., 2014), were less abundant in the cRGC cell pool than in the ipRGC pool. However, the data suggest that contamination in the cRGC pool was not uniform across retinal cell types. Amacrine-specific transcripts were no more abundant overall in cRGCs than in ipRGCs, and microglial and vascular markers were essentially absent, as in ipRGCs.

In immature mice (P5; *Opn4-GFP*), contamination of cRGC samples by non-RGC transcripts appeared more modest than in adults. The major sources of contamination (rods and

Müller glia) are still being born and undergoing early-stage differentiation at this age, and this would presumably depress the abundance of their cell-type-specific transcripts (Young, 1985; Morrow et al., 1998; Matsushima et al., 2011).

To summarize, this analysis suggests that the ipRGC samples were relatively free of contamination by most other retinal cell types. In contrast, contamination of the cRGC samples appears to derive mainly from Müller cells and strongly expressed genes in rods. Though this must be factored into the analysis, our primary focus was on genes more strongly expressed in ipRGCs than in cRGCs, and this difference seems unlikely to be affected by the modest contamination of the cRGC pool.

Genes differentially expressed in ipRGCs

Comparing the abundance of transcripts in the ipRGC and cRGC pools, we identified over 75 genes that were differentially elevated expression in ipRGCs (as marked by one or both melanopsin-reporter lines) relative to cRGCs. Briefly, identification of differentially expressed genes (DEGs) in ipRGCs relied on the following stringent criteria: 1) low FDR with high fold-change, 2) corroboration of differential expression across both ipRGC reporters, and 3) absence of gene expression in cRGC samples (see Methods). Some instances of genes with borderline FDR in a subset of samples, such as *Zcchc12* and *Hs6st2*, were included after closer manual inspection of aligned reads determined relative high expression in ipRGCs combined with absent or relatively low aligned reads in cRGC samples. The identified DEGs are diverse, and most have not been previously identified as ipRGC-enriched (Figure 6; see Methods). Here, we survey some of these genes, grouped by their functional features (Figure 6).

1. ***Transcription factors***

Transcription factors, by regulating other genes, help to generate and maintain ipRGC identity. We noted above that the T-box transcription factor *Tbr2* was much more strongly

expressed in adult ipRGCs than in cRGCs, as expected (Sweeney et al., 2014). *Tbr2* is best known for its key role in early retinal development. Its expression in adult retina is far more restricted, but it remains expressed in the majority of ipRGCs. A second T-box transcription factor, *Tbx20*, was similarly enriched (Figure 6). *Tbx20* has not been previously linked to adult retinal function, but we will show that it too is quite selectively expressed in ipRGCs. Additionally, four other transcription factors, *Irx6*, *Dmrtb1*, *Nr4a3*, and *Pou6f2,* were differentially expressed in adult ipRGCs. Most of these genes serve as broad lineage determinants in early retinal development (Zhou et al., 1996; Star et al., 2012). Other highly expressed genes included the neuron-derived orphan receptor 1 *Nor1* (*Nr4a3*), which codes for a nuclear receptor, and *Elavl2* gene, which codes for a RNA-binding protein important for mRNA metabolism and neuronal differentiation (Fornaro et al., 2007; Hinman and Lou, 2008). Pathway analysis (DAVID) of DEGs in ipRGCs suggested specialization in heparan sulfate biosynthesis, including *Hs3st4*, *Hs3st2*, *Hs6st2*, *Ndst4*, and *Gpc5* (Figure 6).

2. ***Receptors and channels***

Multiple genes encoding diverse surface receptors were differentially expressed in ipRGCs (Figure 8). For example, expression data suggest that ionotropic nicotinic acetylcholine receptors in ipRGCs may be composed of α3, α4, α6, β2 and β3 subunits (Figure 8), although the α3 and α4 transcripts were borderline for differential expression in ipRGCs. In agreement with previous studies, we found that ipRGCs expressed the Drd1 dopamine receptor, but had low levels of Drd2 expression (Van Hook et al., 2012). Several serotonin receptor genes (Htr1b, Htr1d, and Htr5a) were modestly enriched in ipRGCs. The ipRGCs were also found to express many glutamate receptors subunits, but only one of these - the NMDA receptor subunit 3A (GRIN3A) - was differentially expressed relative to other adult RGCs. The mu opioid receptor gene *Oprm1* is differentially expressed in ipRGCs; it could regulate their light responses interacting with L-type calcium channels, which carry the majority of light-evoked inward calcium

current in ipRGCs (Moises et al., 1994; Diaz et al., 1995; Doğrul et al., 2001; Hartwick et al., 2007). Recently, μ-opioid receptors (MOR) immunoreactivity was identified on rodent M1-M3 ipRGCs and MOR activation reduced ipRGC excitability via modulation of voltage-gated potassium and calcium currents (Cleymaet et al., 2019). Our data appear at odds with earlier reports that M1 and M4 ipRGCs express the melatonin receptor genes Mtnr1a and Mtnr1b (Sengupta et al., 2011; Pack et al., 2015; Sheng et al., 2015). Additionally, *Kcnh1*, also known as ether-a-go-go (*Eag1*), was differentially expressed in ipRGCs (Figure 6). Kcnh1 is a voltage-gated K+ channel that has been shown to be crucial for the generation of dark current in the inner segment of rods (Frings et al., 1998), but may normally regulate other neuronal functions in ipRGCs (Martin et al., 2008).

3. ***Cell adhesion***

Genes encoding for several cell adhesion molecules were differentially expressed in ipRGCs (Figure 9B). For example, the cell adhesion molecule *DscamL1* was relatively low in ipRGCs during postnatal development, but the closely related genes encoding the immunoglobulin superfamily (IgSF) adhesion molecules *Sidekick-1* and *Sidekick-2* were enriched in developing ipRGCs. *Unc5a* and *Unc5d* were significantly differentially expressed both in early postnatal and adult ipRGCs. In contrast, expression of *Unc5b* and *Unc5C* in ipRGCs was low relative to that in cRGCs. As suggested previously, expression of the repulsive ligand *Sema6a* was significantly lower in ipRGCs than cRGCs during postnatal development (Matsuoka et al., 2011). However, its receptor *PlxnA4* was enriched in P5 ipRGCs. Another semaphorin, *Sema5a*, was also significantly enriched in developing ipRGCs. Other differentially expressed cell-adhesion molecules *Salm5* (*Lrfn5*), *Clstn2*, *Thbs1*, *Lrrtm2*, *Pcdh19*, *Ptprm*, and *Lrrc4c (Ngl1)* could play significant roles in the formation of ipRGC synapses (Burden-Gulley and Brady-Kalnay, 1999; Lin et al., 2003; de Wit et al., 2009; Xu et al., 2010; Lipina et al., 2016;

Pederick et al., 2016; Lin et al., 2018). The cell surface glycoprotein *Mdga1* was also differentially expressed in developing ipRGCs, and is known to influence the formation and maintenance of inhibitory synapses (Pettem et al., 2013).

4. ***Tolerance to stress***

There is increasing evidence that ipRGCs are resistant to stress and able to survive under circumstances that are fatal for other retinal neurons (Li et al., 2008; de Sevilla Müller et al., 2014; Cui et al., 2015; Duan et al., 2015). The harsh dissociation and FACS processing has the potential of generating stress-induced gene expression changes (Figure 6). We attempted to identify potential survival molecular programs that are specific to ipRGCs compared to generic RGCs. The genes *Adcyap1* (PACAP), *Igf1*, and *Spp1* (*osteopontin*), all of which have previously described roles in promoting ipRGC survival (Atlasz et al., 2010; Duan et al., 2015) were differentially expressed in ipRGCs. We also identified a number of genes related to glial function differentially expressed in ipRGCs, including *Gldn*, *Cntn2*, *Lama4*, and *Astn2*, and *Thbs1* (Figure 6).

5. ***Phototransduction***

Photoactivation of melanopsin photopigment typically triggers a phosphoinositide signaling cascade resembling that in rhabdomeric (invertebrate) photoreceptors, involving G proteins in the Gq family, phospholipase C, and canonical TRP channels. In ipRGCs, the phototransduction cascade typically signals through Gq-family proteins and phospholipase C beta 4 (PLCB4) to open canonical TRP channels (Trpc7 and Trpc6) (Graham et al., 2008; Xue et al., 2011; Hu et al., 2013; Emanuel and Do, 2015; Emanuel et al., 2017) (Figure 10A). Additionally, M2 and M4 ipRGCs use distinct ciliary phototransduction pathway components, including cyclic nucleotide as the second messenger and HCN as the ion channel for phototransduction (Jiang et al., 2018). Further, contrast sensitivity of M4 cells is enhanced by

492 Opn4 phototransduction through the regulation of potassium leak channels (Sonoda et al.,
493 2018).

494 We determined that the genes in this signaling cascade (*Opn4*, *Trpc7*, *Trpc6*, *Plcb4*, and
495 several Gq genes) were expressed at relatively high levels in all three ipRGC pools (i.e.,
496 selective-postnatal; selective-adult; or pan-subtype adult). Moreover, two key genes - *Opn4* and
497 *Trpc7* - were more highly expressed in ipRGCs than in cRGCs in all three ipRGC pools. *Trpc6*
498 was also significantly overexpressed in ipRGCs in younger animals, with a trend in this direction
499 also in adult ipRGCs, but *Trpc7* was expressed at much higher levels than *Trpc6*. Plcb4
500 appears essential for melanopsin phototransduction in some cells, and it was expressed at
501 much higher levels than Plcb1, 2 or 3. However, Plcb4 was differentially expressed in postnatal
502 age ipRGCs compared to cRGCs, but had similar expression during adulthood.

503 Recent evidence indicates that multiple the Gα subunits of the Gq family, including
504 Gnaq, Gna11, or Gna14 subunits, redundantly contribute to phototransduction in ipRGCs
505 (Hughes et al., 2015). Our studies suggest a similar expression pattern, including a lack of
506 Gna15 expression (Figure 10B). Further, we determined that Gna14 was differentially
507 expressed in our P5 ipRGC samples, but it did not reach a statistical significant difference in
508 adult Opn4-GFP ipRGCs. Gnaq appears to be among the highest expressing Gq/11 subunits in
509 our study, which conflicts with the negative finding of Siegert and colleagues (2012). To date,
510 the Gβγ complex involved in the ipRGCs signaling cascade remains unknown. Our studies
511 determined that the beta subunit Gnb1 is by far the most highly expressed in ipRGCs, having a
512 15-fold higher expression than the other subunits Gnb2, Gnb4, or Gnb5; Gnb3 was not
513 detectably expressed in adult ipRGCs (Figure 10C). Additionally, we found that the gamma
514 subunit Gng4 is differentially expressed in ipRGCs.

515 Also differentially expressed in ipRGCs were two factors with known roles in
516 diacylglycerol (DAG) signaling, Ras guanyl nucleotide-releasing protein 1 (*Rasgrp1)* and

517 Diacylglycerol kinase gamma (*Dgkg*) (Figure 10B). *Rasgrp1* is a guanine nucleotide exchange
518 factor (GEF) that activates *Ras* by facilitating its GTP binding (Bivona et al., 2003). Rasgrp1
519 binds DAG and Ca^{2+}, both of which are elevated by melanopsin phototransduction. This
520 provides a possible basis for intrinsic photoresponses of ipRGCs to modulate Ras signaling and
521 thus genes governing cell growth, differentiation and survival. We will return to a more detailed
522 consideration of Rasgrp1 later in this report.

523 *Dgkg* converts DAG to phosphatidic acid, thus acting as a terminator of DAG signaling
524 (Bivona et al., 2003; Shulga et al., 2011). Because DAG appears to be a key link between early
525 steps in phototransduction and gating of the light-activated channels, Dgkg may regulate the
526 kinetics of the photoresponse in ipRGCs. The protein products of the two overexpressed genes
527 may interact. Diacylglycerol kinases are also known to bind to Rasgrp and modulate its activity
528 (Topham and Prescott, 2001). Diacylglycerol and calcium are also known to activate the protein
529 kinase C (PKC) family members Prkcd and Prkcq (Oancea and Meyer, 1998), which we
530 determined to be differentially expressed in ipRGCs. Protein kinase C (PKC) activity has been
531 suggested to be important for deactivating TRPC activity in the invertebrate photoreceptors and
532 potentially also for the Opn4 phototransduction cascade (Graham et al., 2008). Peirson and
533 colleagues (2007) previously identified another PKC member, Prkcz, as being important for
534 ipRGC-mediated photoentrainment of circadian rhythms (Peirson et al., 2007). However, Prkcz
535 is only moderately expressed in ipRGCs in our data, at levels and similar to those in cRGCs.

536 In other photoreceptors, RGS (Regulator of G protein signaling) proteins play a key role
537 in terminating the photoresponse by accelerating the intrinsic GTPase activity of the cognate G-
538 protein (e.g., transducin in rods). Two RGS genes were overexpressed in all three ipRGC pools:
539 *Rgs4* and *Rgs17*. At least one of these (Rgs17) regulates Gq signaling (Mao et al., 2004; Ji et
540 al., 2011) (Figure 10B).

541 The arrestins also contribute to response termination by binding to phosphorylated
542 opsin. ipRGCs exhibited strong expression of both beta arrestin genes (Arrb1, Arrb2) but low

543 expression of rod (*Sag*) and cone (*Arr3*) arrestin genes. This is consistent with earlier evidence
544 that beta arrestins rather than conventional retinal arrestins bind photoactivated melanopsin in
545 ipRGCs (Cameron and Robinson, 2014; Mure et al., 2018). Still, these beta arrestin transcripts
546 are both at similarly high levels in cRGCs as in ipRGCs, presumably because these arrestins
547 regulate diverse GPCRs (Figure 10B).

548 Many of the genes involved in rod and cone phototransduction had low expression
549 (scarce or no read alignment) and/or were present at much lower levels in ipRGCs than cRGCs.
550 These include the genes for opsins, transducin alpha, and arrestin in rods (*Rho*, *Gnat1, Sag*)
551 and cones (*Opn1mw, Opn1sw, Gnat2,* and *Arr3*; Figure 10C). Although Cngb1 was differentially
552 expressed in ipRGCs, the total reads aligning to the Cngb1 locus were low and derived mainly
553 from a limited region of the gene, and the obligatory alpha subunits were not detected, so this
554 could be a false positive (Figure 10C).

555

556 **Genes differentially repressed in ipRGCs**

557 The lack of contamination by non-RGC retinal neurons in the postnatal day 5 (P5)
558 samples allowed us to identify genes that were differentially repressed in ipRGCs compared to
559 cRGCs in early postnatal development. Our data suggested that the transcription factor *Jun*
560 (Jun Proto-Oncogene) and *Irx4* are differentially repressed in P5 ipRGCs samples (Figure 9).
561 Other genes that were differentially repressed in the P5 ipRGC samples included *Satb1*, *Satb2*,
562 and *Foxp2*, all of which are known to have restricted expression in the abundant F-RGC type
563 that is likely included in the cRGC samples (Rousso et al., 2016). The *Pou4f1* (*Brn3a)* and
564 *Pou4f3* (*Brn3c*) transcription factors were both differentially repressed in P5 ipRGCs, consistent
565 with their known lack of expression in ipRGCs (Jain et al., 2012) (Figure 9). The transcriptional
566 repressors *Bcl11b (CTIP2)*, *Irx4*, and *Tbr1* were all found to be differentially repressed in ipRGC
567 compared to cRGCs samples. Furthermore, the *Cdkn1c* (*p57KIP2),* a gene known to be

transcriptionally repressed by Bcl11b (Topark-Ngarm et al., 2006), had relatively increased expression in ipRGCs (Figure 6).

Expression differences between the *Opn4-GFP* and *Opn4-Cre/GFP* reporter systems

To study gene expression differences across the different ipRGC subtypes, we compared the expression patterns of *Opn4-Cre/GFP* (labels M1-M6 subtypes) and *Opn4-GFP* (labels only the M1-M3 subtypes) (Figure 7). In general, genes differentially expressed in ipRGCs identified in the two reporter systems were both supportive and cross-correlated. However, we identified 24 genes that were differentially expressed in the adult *Opn4-Cre/GFP* reporter but had low or no apparent expression in the *Opn4-GFP* reporter, suggesting selective expression in one or more of the M4-M6 ipRGC subtypes. The *Opn4-Cre/GFP* specific genes included *Anxa2*, *Gem*, *Sema3d*, *Rbp4*, and *Rxrg*. Recently, an Rpb4 reporter (Rbp4-Cre) was demonstrated to mark amacrine cells coupled to ipRGCs, although there was an apparent lack of labeling in ipRGCs (Sabbah et al., 2017). The Kcnk4/TRAAK, another gene that was differentially expressed in the *Opn4-Cre/GFP* reporter, encodes a two-pore potassium channel subunit (Fink et al., 1998). Additionally, our data suggest that the Kcns3 electrically silent voltage-gated potassium channel subunit has its expression restricted to the ipRGCs labeled by *Opn4-Cre/GFP*, but this difference did not reach statistical significance (FDR 0.13). However, close inspection of reads aligning to Kcns3 using the integrated genome viewer (IGV) confirmed weak expression in ipRGCs and absent expression in cRGCs for *Opn4-Cre/GFP* samples (data not shown). Lastly, the neurexophilins Nxph1 and Nxph3 were differentially expressed in the *Opn4-GFP* and *Opn4-Cre/GFP* reporters, respectively (Figure 7). These proteins are known to bind α-neurexins in mice and have restricted expression patterns (Missler et al., 1998; Beglopoulos et al., 2005; Craig and Kang, 2007).

Rasgrp1 is selectively expressed in ipRGCs

Since differential mRNA expression does not guarantee a correspondence with protein product (Koussounadis et al., 2015), we sought to test our transcript-level differential expression analysis at the protein level and to determine whether their expression is selective for particular adult ipRGC subtypes. Transcriptional profiling suggested that Rasgrp1 is expressed differentially, possibly even selectively, in ipRGCs. Rasgrp1 has both a calcium and a diacylglycerol binding domain and has well-described role in lymphocytes as a Ras GEF, a nucleotide exchange factor activating Ras through the exchange of bound GDP for GTP activating Erk/MAP kinase. The phototransduction cascade in ipRGCs elevates DAG and intracellular calcium, both of which mediates the Ras GEF activity of Rasgrp1 cascades (Bivona et al., 2003). Therefore, Rasgrp1 is well-positioned to provide a unique form of Ras signaling to a subset of ipRGCs.

We used immunofluorescence against Rasgrp1 (Puente et al., 2000) to label the Rasgrp1 protein in whole-mount retinas from adult wild type mice. Rasgrp1-immunopositive somata were present in the ganglion cell layer (GCL) and in the inner nuclear layer (INL). The latter likely represent amacrine cells or displaced ganglion cells, judging by their close proximity to the inner plexiform layer (IPL) (Figure 11). Immunolabeling marked the cytoplasm as well as the somatic plasma membrane of these cells. Occasionally, particularly strongly Rasgrp1-labeled cells had some dendritic labeling. Rasgrp1 immunostaining was also observed in a subset of photoreceptors in the outer retina (data not shown).

To test whether the Rasgrp1-positive cells in the ganglion-cell layer were RGCs, we carried out double immunofluorescence for both Rasgrp1 (antibody m199) and the RNA-binding protein Rbpms, which selectively labels all and only RGCs (Rodriguez et al., 2014). About half of Rasgrp1-immunopositive cells in the GCL were RGCs, as determined by co-labeling for Rbpms (56%, n = 708 across three retinas, three mice; Figure 11A). Most of these Rasgrp1-expressing RGCs were ipRGCs, as revealed by their immunoreactivity for melanopsin (95.9±1.1%, n = 412, Figure 11A). In contrast, only a fraction of Opn4-immunopositive ipRGCs

were Rasgrp1 immunopositive (34%, *n* = 1169). The remainder of the Rasgrp1-immunopositive cells that are immunonegative for Rbpms (non-RGCs), expectedly, lack Opn4-immunoreactivity and can be assumed to be displaced amacrine cells. Thus, Rasgrp1 expression in the GCL is apparently restricted to a subpopulation of ipRGCs and many amacrine cells.

We next tested whether the immunolabeling of RGCs represented endogenous Rasgrp1 protein expression. The antibody used in this study has been previously shown to specifically label Rasgrp1 protein expression in hippocampal neurons (Pierret et al., 2000). As a further test for the specificity of the antibody, we compared immunofluorescence labelling of whole mount retinas from normal and Rasgrp1-knockout mice generated by inserting *LacZ* and a *Neo* cassette into the Rasgrp1 gene to disrupt its expression (Dower et al., 2000). Our control experiments showed that the GCL and INL cellular immunolabeling is absent in the Rasgrp1 knockout (Figure 11B). However, vasculature and photoreceptor cell labeling persisted in Rasgrp1-knockout mouse retinas, suggesting cross-reactivity of antibody with other proteins.

Rasgrp1 expression is restricted to diverse ipRGC subtypes

We next determined which of the established morphological subtypes of ipRGCs express Rasgrp1 into adulthood (Figure 11C). For this purpose, we used key characteristics such as relative Opn4 expression, soma size, and dendritic morphology. In the GCL, the majority of M1/M3 cells (71.6±3.9%, *n* = 300 M1/M3 across three retinas, three mice), but only a fraction of M2 cells (23.4±5.4%, *n* = 389 M2 cells) expressed Rasgrp1 (Figure 11C). Additionally, many cells with low Opn4-immunofluorescence (designated “low Opn4-IF”) also expressed Rasgrp1 (31.4±6.13%, *n* = 138). Within the INL, displaced M1 cells express Rasgrp1 at a similar percentage as conventionally placed M1 cells (70.7±8.0%, *n* = 3 retinas). We found no examples of Rasgrp1 immunoreactivity in M4 cells (0%, *n* = 172, Figure 11C). Of the Rasgrp1-expressing ipRGCs, half were M1/3 cells (52.8±3.8%), nearly a quarter were M2 cells

(21.1±2.7%) and a small percent (10.4±1.8%) were low Opn4-IF cells (*n* = 396 Rasgrp1^{+}/Opn4^{+} cells across three retinas, three mice) (Figure 11D). Therefore, Rasgrp1 is selectively expressed in a diverse set of ipRGC subtypes.

Tbx20 is expressed in a diverse subset of ipRGCs

The T-box transcription factor Tbx20 was suggested from our gene expression analysis to be differentially expressed in ipRGCs. We selected it for further analysis in part for its potential role in maintaining the adult identity of ipRGCs. Tbx20 co-localization analysis with ipRGC subtypes was characterized as with our previous studies, but with the exception that M3 were combined with M2 types during ipRGC classification (annotated "M2/M3") instead of with M1 types as in our other colabeling studies. Immunofluorescence co-localization analysis of Tbx20 and Opn4 expression confirmed its high expression in a subset of ipRGCs (Figure 12). Tbx20 was expressed in most M1 cells (82.6±1.8%, n=514 across four retinas), but only in a minority of M2/3 cells (30.2±6.5%, n=1305) and low Opn4-IF cells (12.4±3.4%, *n* = 603). Half of the displaced M1 (dM1) cells expressed Tbx20 (46.0±7.1%, *n* = 153). Strikingly, however, Tbx20 was not expressed at all in M4 cells (0%, *n* = 283).

Many Tbx20 cells were not detectably immunopositive for Opn4. Only 41% of Tbx20 immunopositive were also Opn4-immunoreactive (18.5±2.6% were M1 cells; 16.0±2.0% were M2/3 cells; and only 3.6±0.9% were low Opn4-IF cells; *n* = 2184 across four retinas; Figure 13). The remaining Tbx20-immunopositive cells were RGCs, as confirmed by Rbpms-immunoreactivity (data not shown). Additionally, Tbx20-immunopositive RGCs that were also Opn4-immunonegative were topographically enriched in the ventral retina, with most Tbx20-positive cells in the dorsal retina being accounted for by Opn4-immunoreactivity. These results demonstrate that Tbx20 is expressed in a diverse set of RGCs, including ipRGC subpopulations.

Tbx20 expression in M5-M6 ipRGCs

To investigate whether some or all of the Tbx20-immunopositive RGCs that were Opn4-immunonegative might be ipRGCs of the M5 and M6 subtypes that exhibit weak Opn4 immunostaining, we examined the co-localization of Tbx20-immunopositive cells, Opn4-immunopositive cells, and all GFP-labeled cells in the *Opn4-Cre;Z/EG* mouse reporter, which among other ipRGCs, labels M5 and M6 cells. We observed examples of Tbx20-immunopositive cells that were GFP-positive (M1-M6 ipRGCs), but not Opn4-immunopositive M4-M6, and relatively small (not M4), suggesting that Tbx20 may be expressed in at least a subset of M5 or M6 ipRGCs (Figure 13A,B).

To test the implication that many Tbx20 cells were M5 or M6, we turned to Cdh3-GFP mice. Most GFP+ RGCs in this mouse line are M6 cells and the remainder are M5 cells (Quattrochi et al., 2019). We tested Tbx20 immunoreactivity in the context of Opn4 immunofluorescence and *Cdh3-GFP* labeling (Figure 12B,C). For the purpose of this study, we focused on GFP cells in the GCL that are Opn4-immunonegative (to distinguish from Opn4-immunopositive M2 types). We found that at three weeks after birth, most *Cdh3-GFP* cells express the Tbx20 protein (82.1±4.3%, *n* = 439 across four retinas, Figure 12C). Many, but not all, of the Opn4-immunonegative Tbx20-positive cells were GFP^+ (27%, n=1277 $Tbx20^+$;$Opn4^-$ cells; 4 retinas). The dorsal-ventral gradient of Tbx20-positive cells that are Opn4-immunonegative was broadly similar to the retinal labeling of the *Cdh3-GFP* reporter. A large portion of Tbx20-immunopositive cells remained unclassified (43.3±3.8%, n=2184; Figure 13D).

Further, we determined whether Tbx20 expression correlates with the related T-box transcription factor Tbr2, a gene previously described to be enriched in adult ipRGCs (Mao et al., 2014; Sweeney et al., 2014). All Tbx20-expressing cells were strongly Tbr2-immunopositive (*n* = 328; 4 regions distributed across a single adult *Opn4-Cre/GFP* retina; Figure 13C).

Therefore, whereas Tbr2 is expressed in a broad range of types that includes the entire ipRGC family, Tbx20 expression is confined to a diverse subset of ipRGC subtypes.

Molecular diversity of Rasgrp1 and Tbx20 expression in ipRGCs

Our expression studies revealed that Rasgrp1 and Tbx20 have a strikingly similar pattern of expression among ipRGC subtypes. Both genes were expressed in the majority of M1 cells, a minority of M2 cells, and a small population of low Opn4-IF cells, but not in M4 cells (Figures 12 and 14). To directly test for co-expression, we compared and contrasted the expression patterns of Tbx20- and Rasgrp1-immunoreactivity in the context of the M1-M4 subtypes revealed by Opn4-immunoreactivity (Figure 14). Rasgrp1 co-expression with Tbx20 was only observed in a fraction of M1/3 cells (26.0±1.8%; *n* = 241 across two retinas, two mice; Figure 14). Further, M1 cells expressing either Rasgrp1 or Tbx20 alone accounted for roughly similar fractions of M1 cells (37.3±4.0% and 31.1±3.5%, respectively). Only a small fraction of M1 cells were immunonegative for both Rasgrp1 and Tbx20 (5.3±0.7%). In contrast, half of M2 cells lacked Rasgrp1 and Tbx20 immunoreactivity (57.7±3.3%; *n* = 388 across two retinas, two mice). Approximately a third of M2 cells expressed Tbx20 (31.0±0.7%), while only 11.3±5.1% expressed Rasgrp1. We did not observe any example of an M2 cell expressing both Rasgrp1 and Tbx20.

Molecular diversity of SCN-projecting ipRGCs

We further examined the Rasgrp1- and Tbx20-expressing ipRGC subtypes to seek intersectional expression patterns that would divide ipRGCs by their downstream visual pathways. Earlier studies showed that M1 cells could be subdivided based on their level of expression of Brn3b (Chen et al., 2011; Jain et al., 2012). We used quadruple immunolabeling to simultaneously test Brn3b expression with Rasgrp1- and Tbx20-immunoreactivity in the

720 context of Opn4-immunolabeled ipRGCs (25 regions, three wild type retinas; Figure 14A,B). We
721 determined that a minority of M1/3 cells express Brn3b (7.9±6.0%, n=241), which is similar to
722 previous studies (Jain et al., 2012). The Brn3b$^+$ M1/3 cells expressed either Tbx20 or Rasgrp1
723 (91.0 and 9.0±10.1%, respectively; n=30) (Figure 14C).

724 Further, we determined that most M2 cells expressed Brn3b (90.8±6.9, n=168). In
725 contrast to M1/M3 ipRGCs, the majority of Brn3b$^+$ M2 ipRGCs did not express either Rasgrp1 or
726 Tbx20 (67.4.6±13.8, n=222). Most M2 cells expressing Tbx20 were also Brn3b immunopositive
727 (84.5±25.1, n=118). The small subset of M2 cells that express Rasgrp1 could be further divided
728 by Brn3b presence or absence (5.0±6.0% and 4.5±1.4%, respectively; n=168). Generally, we
729 found no cells co-expressing all three genes (n=729).

730 Although Brn3b has been used as a proxy for distinguishing M1 ipRGC subpopulations
731 targeting distinct brain regions, many M1 cells have transient Brn3b expression in development
732 that is downregulated by adulthood (Chen et al., 2011). Therefore, we directly correlated gene
733 expression of Rasgrp1 and Tbx20 in the retina with retrograde labeling from the SCN (Figure
734 15A). We injected rhodamine-conjugated retrobeads in the SCN, followed by
735 immunofluorescence labeling for Opn4, Rasgrp1, and Tbx20 (Figure 15A-C). All injection sites
736 clearly involved the SCN, as revealed by DAPI labeling, but did not spread to the optic chiasm
737 or tract (Figure 15B). Quantitative co-expression analysis (18 confocal images collected across
738 the contralateral and ipsilateral retinas) revealed that nearly all retrolabeled cells were Opn4-
739 immunopositive (95.2%, 248 retrolabeled cells). Most retrolabeled Opn4-immunoreactive cells
740 expressed both Rasgrp1 and Tbx20 (79±5%, across 18 sections, 235 cells), but equal minorities
741 expressed either Rasgrp1 (10±3%) or Tbx20 (10±4%, Figure 15C). This expression pattern was
742 consistent across the ipsi- and contralateral retina (Figure 15D), as suggested by a bilateral
743 input to the SCN (Hattar et al., 2006; Fernandez et al., 2016). Therefore, we show that SCN-

744 projecting ipRGCs have a complex pattern of Rasgrp1 and Tbx20 gene expression. Together,
745 these results provide evidence for previously unrecognized molecular diversity in adult ipRGCs.
746
747 **Discussion**
748 Prior efforts to assess the distinctive genetic composition of ipRGCs have been complicated by
749 their rarity among diverse retinal cell types and the inherent difficulties of maintaining viability of
750 dissociated mature neurons (Lobo et al., 2006). Our approach was first to isolate RGCs by
751 immunoaffinity, then to further purify ipRGCs from these based on genetic labeling and FACS,
752 and to finally to compare the transcriptional profiles of the purified ipRGCs to those of the
753 residual cell pool, consisting mainly of conventional RGCs. The relative purity of our ipRGC
754 sample is supported by enrichment for transcripts of genes known to be differentially expressed
755 in ipRGCs and the low levels of transcripts selectively expressed in potentially contaminating
756 populations, including the abundant rod photoreceptors. Our isolation method and differential
757 expression analysis allowed us to identify more than 75 DEGs in ipRGCs relative to
758 conventional RGCs.
759
760 **Genes differentially expressed in adult ipRGCs**
761 There is limited knowledge of specific gene expression in ipRGCs generally and within
762 particular ipRGC subtypes, especially non-M1 ipRGCs. Many diverse genes appeared more
763 highly expressed in ipRGCs than in conventional RGCs. We confirmed differential protein
764 expression in ipRGCs immunohistochemically for two of these genes: Tbx20, a transcription
765 factor implicated in visual development; and Rasgrp1, a G-protein exchange factor that may
766 interact with the melanopsin phototransduction cascade. However, only a subset of ipRGCs
767 appeared to express detectable levels of these proteins, and such variable expression was
768 apparent even among ipRGCs of the same subtype. Some ipRGCs expressed both proteins,
769 but many did not. This diversity even extended to the M1 cells projecting to the SCN, which had

been thought to share the distinctive molecular feature of little or no expression of the transcription factor Brn3b. These novel markers of molecularly distinctive ipRGC varieties open the way for cell-type-specific manipulations through intersectional strategies.

What type(s) of adult ipRGCs express Rasgrp1?

Rasgrp1 expression has previously been detected in the hippocampus, striatum and olfactory regions of the brain (Ebinu et al., 1998; Toki et al., 2001), but our study appears to be the first to explore Rasgrp1 expression in the eye. Rasgrp1-like immunoreactivity marked a diverse subpopulation of ipRGC subtypes, including the M1-M3 ipRGC subtypes but not the M4-type. Either M5 or M6 ipRGCs, or both, also appear likely to express Rasgrp1, because some Rasgrp1 immunoreactive cells had weak Opn4-immunoreactivity without the characteristic dendritic labeling of M1-M3 ipRGCs and with somas too small to be M4 cells (Ecker et al., 2010; Quattrochi et al., 2019; Stabio et al., 2018).

We find Rasgrp1 to be expressed not only in SCN-projecting M1 ipRGCs, but also in other ipRGC subtypes, especially M2 cells and apparently M5 and/or M6 cells. Collectively, these types project to various non-image-forming visual centers, including the olivary pretectal nucleus, intergeniculate leaflet, and dorsal lateral geniculate nucleus (Quattrochi et al., 2019; Stabio et al., 2018).

The function of Rasgrp1 in ipRGCs is unknown, but it could interact with the melanopsin phototransduction cascade. The direct photoresponse of ipRGCs appears to increase levels of both DAG and calcium. Both of these signaling molecules bind to and activate Rasgrp1, and trigger its translocation to the Golgi apparatus (Bivona et al., 2003; Graham et al., 2008; Zhang et al., 2010). However, ipRGC phototransduction Rasgrp1 signaling does not appear to be essential for ipRGC phototransduction because more than a quarter of M1 ipRGCs and the great majority of M2 cells are immunonegative for Rasgrp1. Even in ipRGCs, Rasgrp1 may be activated by DAG and calcium signals unrelated to Opn4 phototransduction, and such signals

796 are presumably also responsible for modulating Rasgrp1 in cells (such as certain amacrine
797 cells) which express Rasgrp1 but not melanopsin.

798 Rasgrp1 has the potential to affect any number of neuronal signaling pathways. Ras
799 signaling pathways are enormously complex and the cross talk between pathways makes it
800 even harder to identify specific effects. One basic mechanism for specificity in Ras signaling is
801 the distinct subcellular targeting of downstream components of the signaling pathway. In
802 lymphocytes, localized Ras signaling of Rasgrp1 occurs preferentially on the Golgi apparatus,
803 which is a rare form of compartmentalized Ras signaling (Bivona et al., 2003; Zhang et al.,
804 2010). The Golgi apparatus in neurons provides the posttranslational protein modifications
805 required for organizing protein and organelle trafficking throughout the cell. Rasgrp1 could play
806 a crucial role in orchestrating a specific set of post-translational modifications at the Golgi.
807
808 **Tbx20 is expressed in a diverse set of ipRGC subtypes**
809 The T-box transcription factor Tbx20 exhibited enriched expression relative to
810 conventional RGCs in postnatal and adult retinas. Double immunolabeling revealed that many
811 ganglion cells that expressed this protein also expressed melanopsin. Similar to Rasgrp1,
812 Tbx20 was determined to be expressed in most M1 ipRGCs (83%), a substantial minority of M2
813 cells (30%) and an additional population of RGCs whose identity was not immediately obvious.
814 We decided to then compare Tbx20 against other known molecular patterns in ipRGCs.
815 Whereas most RGCs follow a Brn3b-dependent developmental program, the M1 ipRGCs that
816 project to the SCN do not express Brn3b while OPN-projecting M1 ipRGCs express Brn3b. We
817 found that Brn3b-expressing M1 cells are also Tbx20-immunopositive. The Brn3b-negative M1
818 cells are split between cells that express Tbx20 and those that do not. This finding suggests that
819 ipRGCs are more molecularly diverse than originally anticipated: Tbx20 is expressed in ipRGCs
820 with differing brain targets, Tbx20 is expressed across multiple morphologically defined

subtypes, and Tbx20 is not expressed in all of any one type. The exploration of Tbx20 coexpression with Rasgrp1 revealed a complex coexpression pattern among M1-M3 ipRGCs.

Tbx20 has well-established roles in embryonic development and is continuously required in mature neurons and other cell types to maintain their identities and functional properties during adulthood (Naiche et al., 2005). Tbx20 functions as a repressor in early embryonic ocular development (Carson et al., 2000; Pocock et al., 2008) and is required for the expansion of the small pool of precursor cells in the optic vesicle (Carson et al., 2004). However, little is known about the function of Tbx20 in the adult retina.

Tbx20 can function as a transcriptional activator in parallel with its repressor activity, with these two roles impinging on distinct biological processes (Sakabe et al., 2012). In addition to its key developmental roles, Tbx20 appears vital for maintaining the structure and function of cardiac muscle cells in the adult mouse heart (Stennard et al., 2003; Shen et al., 2011). In adult cardiomyocytes, Tbx20 is responsible for directly activating genes critical for normal adult cardiac function such as those required for ion transport and heart contraction (Shen et al., 2011; Sakabe et al., 2012). In contrast, genes directly repressed by Tbx20 have known roles in non-heart developmental programs, cell cycle, proliferation, and immune response (Sakabe et al., 2012). The transcriptional effects of Tbx20 shift during cardiac development, from early mediation of proliferation of cardiac progenitors, to implementation of an anti-proliferative program in the adult heart (Cai et al., 2005; Takeuchi et al., 2005). Therefore, Tbx20 cooperates with distinct cohorts of transcription factors to either promote or repress distinct molecular programs in a context-dependent manner (Sakabe et al., 2012). Similarly, binary cell fate specification in the retina is driven by complex genetic programs that require the simultaneous activation and repression of genes by transcription factors. Tbx20 may prove to have a similar reversal in its transcriptional activity in the retina when transitioning from broad embryonic development program to regulating adult neuron identity of a subset of ipRGCs. Further, Tbr2 is another Tbox family member that is known to have a critical role in the development of retinal

847 ganglion cells (Mao et al., 2008), which later becomes essential to a restricted set of ipRGCs
848 that participate in NIF visual circuits (Mao et al., 2014; Sweeney et al., 2014). Our studies
849 determined that Tbx20 and Tbr2 are coexpressed in adult ipRGCs. They may work
850 cooperatively to specify ipRGC subtype identity by regulating cell-specific transcriptional
851 programs and repressing alternate fates.
852
853 **Characterization of ipRGC subtypes**
854 Retinal cell types are generally classified using a combination of morphology, gene
855 expression, mosaic organization, light responses and synaptic connectivity (Sanes and
856 Masland, 2015). By these criteria, intrinsically photosensitive RGCs comprise at least six distinct
857 cell types. Though all express melanopsin, they differ from one another in the strength of the
858 intrinsic response, their morphology, pattern of light responses, and projections to the brain.
859 However, the further subdivision may be in order. The M1 type appears subdivisible into at least
860 two subtypes, one expressing the transcription factor Brn3b and innervating the OPN and
861 geniculate complex, while the other lacks Brn3b expression and innervates the SCN (Chen et
862 al., 2011). Our study shows further diversity in the M1 and M2 types based on the expression of
863 Rasgrp1 and Tbx20. For example, we find molecular diversity among in the SCN-projecting
864 ipRGC subtypes. It is unclear to us whether this should be used to propose a further formal
865 subdivision of M1 and M2 cells. For example, the expression of these proteins could fluctuate
866 over time in individual cells and be uncorrelated across cells of the same type.
867
868 **Comparison with other ipRGC gene expression profiles**
869 Siegert and colleagues (2012) surveyed gene expression in many different sets of
870 mouse retinal neurons, using specific mouse reporters strains (including the *Opn4-Cre* reporter
871 system for ipRGCs), FACS isolation of labeled cells, and microarray analysis. Many of the
872 genes they found strongly expressed in ipRGCs were also among the genes we found

differentially expressed in ipRGCs. However, dozens of additional genes differentially expressed in ipRGCs emerged from our analysis that were not detected in theirs (Siegert et al., 2012). Discrepancies between their findings and ours may stem from technical factors such as differing degrees of contamination of the starting material with rod photoreceptor transcripts, the use of internal control cell populations for relative gene expression comparison in our study but not theirs, and differences between microarray and RNA-sequencing methodologies.

Another study used single-cell transcriptomic analysis of the mouse retina and were able to identify ipRGCs from their cell suspensions (Macosko et al., 2015). Macosko et al., 2015 distinguished the main broad class of RGCs, but they required *post hoc* supervised analysis to distinguish a limited number of genes attributed to Opn4-positive cell clusters. They identified nine genes with a two-fold increase in expression compared to Opn4-negative cells. Three genes (Tbr2, Igf1, and Tbx20) were also found to be enriched in our ipRGC samples. In contrast, Tbx20 did not reach above threshold for Siegert et al., (2012), but it is among the highest expressing ipRGC-enriched genes in our study. Our study complements a recently published single-cell RNA-seq study of RGCs from pre-eye opening age (P5) mice (Rheaume et al., 2018). Although ipRGCs were not a major focus, Rheaume et al., 2018 recognized ipRGCs by clustering and considering established markers such as Opn4 and Eomes/Tbr2 in clusters 6, 25, 26, 33, and 37. They identified further molecular diversity that maps well onto known ipRGC subtypes and those described in our current study. Rheaume et al. determined that the ipRGCs clusters 25 and 37 have major expression of Tbx20, with minor expression in cluster 6. Although not explicitly mentioned, their dataset also includes restricted Rasgrp1 expression in clusters 6 and 25. Considering our gene expression datasets and co-expression studies of Rasgrp1 and Tbx20 in subsets of M1 and M2 cells, we suggest that clusters 6 and 25 constitute these types. Further, we infer that clusters 26 and 37 represent M5 and M6 cells, respectively, considering the following information: 1) Cdh3 expressed in clusters 6, 26, and 37. The *Cdh3-GFP* reporter preferentially labels bistratified M6 ipRGCs, but also labels some monostratified M2 and M5

ipRGCs (Quattrochi et al., 2019); 2) *Cdh3-GFP* labeled RGCs express Cdh6 (Osterhout et al., 2011), which is expressed in clusters 26 and 37; 3) Our study determined that Tbx20 was highly expressed in *Cdh3-GFP* reporter, suggesting enriched expression in M6 ipRGCs. Important differences remain between the experimental parameters of these two studies. Droplet-based scRNA-seq technologies used by Rheaume et al., 2018 provides hierarchies of molecular types and classes, but the sequencing is relatively shallow and our complementary approach of deep sequencing purified populations of ipRGCs generates more complex cDNA libraries with increased sensitivity of detected gene enrichment. In addition to postnatal age group similar to Rheaume et al., we expanded our gene expression profiles to adult ipRGCs, which required substantial optimizations of our dissociation and FACS acquisition process to obtain viable samples of the relatively fragile adult neurons.

Further considerations

Our identification of DEGs in ipRGCs should be treated as hypothesis for genes that are functionally relevant for ipRGC function. Although our selection criteria dramatically decreased the potential heterogeneity obscuring differential gene expression in ipRGC, the transgenic reporters used in our studies are known to label multiple morphologically and physiologically distinct ipRGC types. For example, genes determined to be differentially expressed using the *Opn4-GFP* reporter can, at best, be inferred to have restricted expression within the M1-M3 ipRGC types. However, it would be impossible to know whether this gene is expressed in all M1-M3 types or a subset. Further, we cannot assume that DEGs in our studies are uniquely expressed in ipRGCs and absent in non-ipRGCs. Our studies are based on relative abundance of ipRGCs compared to cRGC populations. As exemplified by Tbx20, we cannot rule out scenarios that DEGs are enriched in ipRGCs, but are also expressed in additional subsets of other RGCs.

The study of transcriptomes and differential gene expression has certainly proven important for revealing otherwise unknown molecular underpinnings to specialized cell function. However, the transcription of genomic DNA to mRNA is only one of many intermediate steps to the synthesis of functional proteins. Translational control, post-translational modifications, and subcellular localizations are examples of ways that the level and function of proteins can be decoupled from the relative abundance of mRNA expression. Therefore, additional follow-up localization studies using *in situ* hybridization or immunofluorescence will be required to test the validity and cell type-specific expression of our proposed DEGs.

Conclusion

In conclusion, our results demonstrate a method to purify ipRGCs and identify an extensive list of more than 75 genes that are differentially expressed in adult ipRGCs compared to generic RGCs. These genes will be useful for the identification of marker genes for ipRGC subtypes, comparison of gene expression across types, understanding the intracellular gene networks underlying ipRGC phenotypes, and the testing for conservation of ipRGC molecular programs across mammalian species.

Figure legends (see attached PDF for figure images)

Figure 1. Experimental design of gene expression profiling from purified ipRGCs and comparison with generic RGCs.

A. Current model of ipRGC family members integrating molecular, physiology, brain circuitry, and morphology (see text for details).

B. Two transgenic reporters were used for gene expression profiling of ipRGCs. The BAC transgenic *Opn4-GFP* labels M1-M3 ipRGCs while the *Opn4-Cre* crossed with a cre-dependent GFP reporter labels M1-M6 ipRGCs. Within the schematic of the gene expression profiling

procedure. 1) Isolation of cell populations from enzymatically dissociated retinas. 2) The surface protein Thy-1 is enriched in RGCs, this high affinity of Thy1-conjugated magnetic beads to RGCs was used to enrich the extracted cell populations with RGCs. 3) Fluorescence-activated cell sorting (FACS) was used to isolate GFP-positive cells (ipRGCs) from GFP-negative cells (cRGCs). These two populations were isolated in parallel to provide direct internal testing of ipRGCs versus cRGCs under the same treatments, conditions, and genetic backgrounds. 4) The RNA of these two main populations was subjected to mRNA extraction. 5) The RNA was converted to cDNA and amplified using Nugen Ovation RNA amplification system. 6) Illumina Truseq sequencing libraries were prepared by ligating adapters to the cDNA. Single-end 50 base pair sequencing was completed using the Illumina HiSeq system. 7) Differentially expressed genes were determined using EdgeR bioinformatics pipeline. See Methods for details.

Figure 2. Characterization of Opn4-based fluorescent reporters for gene expression studies.

A. Immunofluorescence of anti-Opn4 immunofluorescence (IF) of whole mount retina from transgenic *Opn4-GFP* mice with fluorescent protein expression in ipRGCs. Red, Opn4-immunolabeling; green, fluorescently labeled cells; yellow, merged co-localized labeling pattern. Scale bar, 20 μm.

B. Co-expression of *Opn4-Cre/GFP* labeling with immunofluorescence of anti-Opn4 staining of whole mount retina. Red, Opn4-immunolabeling; green, fluorescently labeled cells; yellow, merged co-localized labeling pattern. Scale bar, 20 μm.

C. Quantification of labeling efficiency of Opn4-immunolabeled M1-M3 ipRGCs by *Opn4-Cre/GFP*. Additional comparison of GFP-labeling in low Opn4-expressing ipRGC subtypes M4 (large soma) and M5/6 (small soma).

Figure 3. Fluorescence activated cell sorting (FACS) gating strategy for isolating ipRGCs (GFP+) in parallel with GFP-negative cells that are enriched for RGCs.

A-C. Healthy cells were selected against death marker 7-AAD (not G1). The ipRGCs (GFP^+) and generic RGCs (GFP^-) cells were selected based on intensity and similar relative cell size ultimately using gates G2A and G3A, respectively.

A. Example sort from retina of postnatal day 4 (P4) *Opn4-GFP* mouse.

B. Example sort from retina of young adult *Opn4-GFP* mouse, with noticeably higher debris and cell death.

C. Microscopy testing of accurate sorting of GFP+ cells isolated from P4 *Opn4-Cre/GFP* mouse.

D. Total sequenced reads from adult *Opn4-GFP* and *Opn4-Cre/GFP* reporters.

Figure 4. Scatterplot analysis of relative gene expression and dispersion of biological replicates from positively-selected ipRGCs and enriched conventional RGCs.

A. Volcano plot analysis of gene transcripts with positive fold-change (x-axis; ipRGC-enriched relative to cRGCs) plotted against the negative logarithm of the FDR (y-axis). Significant differentially expressed transcripts (FDR<0.05) are represented as red dots, while transcript with FDR>0.05 have black dots. blue transcripts, Parv-Cre/TdT enriched; red, SNS-Cre/TdT enriched, twofold, $p < 0.05$). The most significant genes from each sample set are attributed with gene name labels, with limits implemented for text readability (FDR<1E-20 and logFC>2 for postnatal age Opn4-GFP reporter ; FDR<1E-4 and logFC>3 for adult ipRGC reporters).

B. EdgeR multi-dimensional scaling (MDS) plot illustrates the overall similarity between expression profiles of different samples. Each sample is denoted by a letter (“i” for ipRGCs; c for cRGCs) and a number, corresponding to particular replicate, comprising one pool of purified RGCs then divided into the two pools. Numbering scheme represents paired ipRGCs (GFP+) and cRGCs (GFP-) replicates (i.e., ipRGC sample ‘i1’ was processed in parallel with cRGC sample ‘c1’, sample ‘i2’ with ‘c2’, etc.). Distances are approximately the log2 fold changes

between samples. Green and gray ovals represent ipRGC (GFP+) and cRGC (GFP-) samples, respectively. Adapted from EdgeR simple graphical output of individual samples in 2D space.

Figure 5. Purity and cell composition assessment of ipRGC and generic RGC samples. Heat map of known cell type marker gene expression in the retina to assess purity and cell composition of ipRGC and generic RGC samples. Shown are biological replicates tested for *Opn4-GFP* (P5 and adult) and *Opn4-Cre/GFP* reporters. Relative expression levels, fold change, and false discovery rate (FDR) are color-coded as indicated in the figure. White boxes indicate high gene expression, while blue represents little or no detected expression. FDR is not available ("NA") in cases that our analysis filtered out genes with very low counts, less than 1 count per million (cpm), in more than half of the samples used in the differential expression analysis.

Figure 6. The expression pattern of candidate ipRGC-specific genes. Heat map of 83 genes differentially expressed in ipRGCs that have functional links to GPCR signaling, regulation and maintenance of molecular programs, neuron communication and organization, neuron survival, and neuron-glia interactions. Relative expression levels, fold change, and FDR are color-coded as indicated in the figure.

Figure 7. Expression pattern differences between Opn4-based reporters. Heat map of genes differentially expressed in adult ipRGCs labeled by the *Opn4-Cre/GFP* reporter (M1-M6 ipRGCs) compared to *Opn4-GFP* (M1-M3 ipRGCs). Relative expression levels, fold change, and FDR are color-coded as indicated in the figure.

Figure 8. The expression pattern of neurotransmitter receptors.

Heat map of genes encoding for nicotinic acetylcholine, dopamine, serotonin, glycine, glutamate, and melatonin receptors. Relative expression levels, fold change, and FDR are color-coded as indicated in the figure.

Figure 9. The expression pattern of developmentally regulated genes in ipRGCs.

A. Heat map of genes encoding transcription factors that have a particular temporal pattern of differential expression in ipRGCs (e.g., high gene expression in P5 ipRGCs relative to adult expression). Relative expression levels, fold change, and FDR are color-coded as indicated in the figure.

B. Heat map of genes relevant for development of ipRGCs. Relative expression levels, fold change, and FDR are color-coded as indicated in the figure.

Figure 10. Phototransduction-related gene expression.

A. Distinct from rod and cone photoreceptors, the light-activation of Opn4 triggers a membrane-bound signaling cascade including $G_{q/11}$ type G-proteins, the generation of 1,2-diacylglycerol (DAG) by PLCβ4, the opening of downstream TRPC6 and TRPC7 channels, and ultimately leads to the influx of calcium through L-type voltage-gated calcium channels.

B. Heat map of genes that are potentially relevant to the Opn4-mediated phototransduction signaling cascade. Relative expression levels, fold change, and FDR are color-coded as indicated in the figure.

C. Heat map of genes previously described to play a role in the light response, dark adaptation, and chromophore regeneration of rod and cone photoreceptors. Relative expression levels, fold change, and FDR are color-coded as indicated in the figure.

Figure 11. Rasgrp1 is selectively expressed in ipRGCs.

A. Whole mount retina immunostained for Opn4, Rasgrp1, and the pan-RGC marker Rbpms (gray-scale). Focal plane is at the ganglion cell layer (GCL). We quantified co-localization of the three markers in confocal images of 49 regions that were topographically dispersed across three whole-mount adult retinas. Co-localization of Rasgrp1 (green), Rbpms (red), and Opn4 (magenta). Rasgrp1 is expressed in a subpopulation of amacrine cells and RGCs (Rbpms-negative and -positive, respectively). Scale bar, 20 µm.

B. Rasgrp1 immunolabeling (antibody sc-8430) of cell bodies in GCL of Rasgrp1$^{+/-}$ heterozygous mice (left, yellow arrows). Absence of cell body immunolabeling in Rasgrp1$^{-/-}$ knockout mice (right) suggests a lack of cellular off-target antibody staining.

C. Quantification of Rasgrp1-expression across Opn4-immunopositive ipRGC subtypes. 70% of M1 and displaced M1 (dM1) cells were Rasgrp1 immunopositive while only 20-30% of either M2, M5 or M6 cells were Rasgrp1 immunopositive. None of the identified M4 cells were Rasgrp1 immunopositive. M1 and M3 types were combined during the process of co-expression analysis (designated “M1/M3”). Error bars represent standard error of the mean.

D. Distribution of all Rasgrp1-expressing RGCs (Rasgrp1^{+};Rbpms^{+}) that belong to specific RGC types, to the extent that could be determined, including Opn4-immunoreactive ipRGC subtypes. No examples of M4 cells were observed to express Rasgrp1. The vast majority (96%) of Rasgrp1-RGCs are Opn4-immunopositive and therefore ipRGCs. The remaining “unknown” RGC types expressing Rasgrp1 (Rasgrp1^{+} ; Rbpms^{+} ; Opn4$^{neg.}$) could be a low-expressing ipRGC type or conventional RGCs. Error bars represent standard error of the mean.

Figure 12. Colocalization study of Tbx20-expression in ipRGC subtypes.

A. Triple immunofluorescence of Opn4, Tbx20, and *Cdh3-GFP* (gray scale).

B. Tbx20-expression in subset of M1-M3 ipRGCs as well as an additional population of Opn4-immunonegative cells.

B,C. Tbx20 is concentrated in the nucleus of most *Cdh3-GFP*-cells.

D. Quantification of Tbx20-expression across Opn4-immunopositive ipRGC subtypes. Tbx20 immunofluorescence labels multiple ipRGC subtypes, including M1s, M2 cells and small soma, low Opn4 expression cells (presumptive M5/M6 ipRGCs), and *Cdh3-GFP* cells (M6-type enriched). M2 and M3 types were combined during the process of co-expression analysis (designated "M2/M3"). Error bars represent standard error of the mean.

Figure 13. Coexpression study of Tbx20 with *Opn4-Cre/GFP* and Tbr2, including distribution of Tbx20-expression across ipRGC subtypes.

A-C. Quadruple immunofluorescence of Opn4, Tbx20, Opn4-Cre/GFP, and Tbr2. Scale bar, 20 μm.

A. Gray scale of Opn4, Opn4-Cre/GFP, and Tbx20 immunofluorescence.

B. Co-expression study of Tbx20 (green) in the context of Opn4 (magenta) and *Opn4-Cre/GFP* (red) labeling. GFP cells that are Opn4-immunonegative are inferred M4-M6 types.

C. Co-expression analysis of Tbr2 (magenta) with Tbx20 (green).

D. Distribution of Tbx20 expressing cells that belong to specific RGC types, to the extent that could be determined, including Opn4-immunoreactive ipRGC subtypes and RGCs labeled by the *Cdh3-GFP* transgenic reporter. Unaccounted Tbx20-expressing cells are designated as "unknown" RGC types. Error bars represent standard error of the mean.

Figure 14. Complex pattern of Rasgrp1-Tbx20-Brn3b co-expression suggests further diversity in ipRGC family.

A. Quadruple immunofluorescence study of Tbx20, Brn3b, Opn4, and Rasgrp1 (gray-scale).

B. Rasgrp1 and Opn4 (left panel) were initially quantified for ipRGC subtype expression prior to comparison with Tbx20 (middle panel) and Brn3b (right panel) expression. Rasgrp1, Brn3b, and Tbx20 expression are partially overlapping.

C. Integrated co-expression patterns of Brn3b, Rasgrp1, and Tbx20 with M1 and M2 ipRGC subtypes. The M1 group includes displaced M1 and M3 types.

Figure 15. The ipRGCs projecting to the suprachiasmatic nucleus (SCN) have a molecularly diverse pattern of Rasgrp1 and Tbx20 expression.

A. Experimental design of fluorescent bead injection to SCN, followed by examination of Rasgrp1 and Tbx20 expression in retrograde labeled RGCs.

B. Neuroannatomical study to verify that retrograde injection is within the SCN, but not the optic nerve.

B. Triple immunofluorescence of Opn4, Rasgrp1, and Tbx20 in combination with fluorescent Retrobeads. Retrobeads were mostly observed in Opn4-immunopositive RGCs (M1-M3 ipRGCs). Quantification of Rasgrp1 and Tbx20 in retrolabeled cells.

D. SCN-projecting ipRGCs in the ipsilateral and contralateral retina are molecularly diverse for Tbx20 and Rasgrp1 expression.

References

Anders S, Huber W (2010) Differential expression analysis for sequence count data. Genome Biology 2010 11:10 11:R106.

Anders S, McCarthy DJ, Chen Y, Okoniewski M, Smyth GK, Huber W, Robinson MD (2013) Count-based differential expression analysis of RNA sequencing data using R and Bioconductor. Nature Protocols 8:1765–1786.

Atlasz T, Szabadfi K, Kiss P, Racz B, Gallyas F, Tamas A, Gaal V, Marton Z, Gabriel R, Reglodi D (2010) Pituitary adenylate cyclase activating polypeptide in the retina: focus on the retinoprotective effects. Ann N Y Acad Sci 1200:128–139.

Barres BA, Silverstein BE, Corey DP, Chun LLY (1988) Immunological, morphological, and electrophysiological variation among retinal ganglion cells purified by panning. Neuron 1:791–803.

Bedont JL, Blackshaw S (2015) Constructing the suprachiasmatic nucleus: a watchmaker's perspective on the central clockworks. Front Syst Neurosci 9:74.

1134 Beglopoulos V, Montag-Sallaz M, Rohlmann A, Piechotta K, Ahmad M, Montag D, Missler M
1135 (2005) Neurexophilin 3 is highly localized in cortical and cerebellar regions and is
1136 functionally important for sensorimotor gating and motor coordination. Mol Cell Biol
1137 25:7278–7288.

1138 Berson DM, Castrucci AM, Provencio I (2010) Morphology and mosaics of melanopsin-
1139 expressing retinal ganglion cell types in mice. Journal of Comparative Neurology 518:2405–
1140 2422.

1141 Bivona TG, Pérez De Castro I, Ahearn IM, Grana TM, Chiu VK, Lockyer PJ, Cullen PJ, Pellicer
1142 A, Cox AD, Philips MR (2003) Phospholipase Cgamma activates Ras on the Golgi
1143 apparatus by means of RasGRP1. Nature 424:694–698.

1144 Brewer GJ (1997) Isolation and culture of adult rat hippocampal neurons. Journal of
1145 Neuroscience Methods 71:143–155.

1146 Brewer GJ, Torricelli JR (2007) Isolation and culture of adult neurons and neurospheres. Nature
1147 Protocols 2:1490–1498.

1148 Brewer GJ, Torricelli JR, Evege EK, Price PJ (1993) Optimized survival of hippocampal neurons
1149 in B27-supplemented neurobasal™, a new serum-free medium combination. Journal of
1150 Neuroscience Research 35:567–576.

1151 Burden-Gulley SM, Brady-Kalnay SM (1999) PTPmu regulates N-cadherin-dependent neurite
1152 outgrowth. J Cell Biol 144:1323–1336.

1153 Cahoy JD, Emery B, Kaushal A, Foo LC, Zamanian JL, Christopherson KS, Xing Y, Lubischer
1154 JL, Krieg PA, Krupenko SA, Thompson WJ, Barres BA (2008) A transcriptome database for
1155 astrocytes, neurons, and oligodendrocytes: a new resource for understanding brain
1156 development and function. J Neurosci 28:264–278.

1157 Cai C-L, Zhou W, Yang L, Bu L, Qyang Y, Zhang X, Li X, Rosenfeld MG, Chen J, Evans S
1158 (2005) T-box genes coordinate regional rates of proliferation and regional specification
1159 during cardiogenesis. Development 132:2475–2487.

1160 Cameron EG, Robinson PR (2014) β-Arrestin-Dependent Deactivation of Mouse Melanopsin
1161 Craft CM, ed. PLoS ONE 9:e113138.

1162 Caretti E, Devarajan K, Coudry R, Ross E, Clapper ML, Cooper HS, Bellacosa A (2008)
1163 Comparison of RNA amplification methods and chip platforms for microarray analysis of
1164 samples processed by laser capture microdissection. Journal of Cellular Biochemistry
1165 103:556–563.

1166 Carson CT, Kinzler ER, Parr BA (2000) Tbx12, a novel T-box gene, is expressed during early
1167 stages of heart and retinal development. Mechanisms of Development 96:137–140.

1168 Carson CT, Pagratis M, Parr BA (2004) Tbx12 regulates eye development in Xenopus embryos.
1169 Biochemical and Biophysical Research Communications 318:485–489.

1170 Chen SK, Badea TC, Hattar S (2011) Photoentrainment and pupillary light reflex are mediated
1171 by distinct populations of ipRGCs. Nature 476:92–95.Clément-Ziza M, Gentien D, Lyonnet

1172 S, Thiery J-P, Besmond C, Decraene C (2009) Evaluation of methods for amplification of
1173 picogram amounts of total RNA for whole genome expression profiling. BMC Genomics
1174 10:246.

1175 Cleymaet AM, Gallagher SK, Tooker RE, Lipin MY, Renna JM, Sodhi P, Berg D, Hartwick ATE,
1176 Berson DM, Vigh J (2019) μ-Opioid Receptor Activation Directly Modulates Intrinsically
1177 Photosensitive Retinal Ganglion Cells. Neuroscience 408:400-417.

1178 Craig AM, Kang Y (2007) Neurexin-neuroligin signaling in synapse development. Current
1179 Opinion in Neurobiology 17:43–52.

1180 Cui Q, Ren C, Sollars PJ, Pickard GE, So KF (2015) The injury resistant ability of melanopsin-
1181 expressing intrinsically photosensitive retinal ganglion cells. Neuroscience 284:845–853.

1182 de Sevilla Müller LP, Sargoy A, Rodriguez AR, Brecha NC (2014) Melanopsin Ganglion Cells
1183 Are the Most Resistant Retinal Ganglion Cell Type to Axonal Injury in the Rat Retina Tosini
1184 G, ed. PLoS ONE 9:e93274.

1185 de Wit J, Sylwestrak E, O'Sullivan ML, Otto S, Tiglio K, Savas JN, Yates JR, Comoletti D, Taylor
1186 P, Ghosh A (2009) LRRTM2 interacts with Neurexin1 and regulates excitatory synapse
1187 formation. Neuron 64:799–806.

1188 Diaz A, Ruiz F, Flórez J, Hurlé MA, Pazos A (1995) Mu-opioid receptor regulation during opioid
1189 tolerance and supersensitivity in rat central nervous system. J Pharmacol Exp Ther
1190 274:1545–1551.

1191 Doğrul A, Yeşilyurt O, Işimer A, Güzeldemir ME (2001) L-type and T-type calcium channel
1192 blockade potentiate the analgesic effects of morphine and selective mu opioid agonist, but
1193 not to selective delta and kappa agonist at the level of the spinal cord in mice. Pain 93:61–
1194 68.

1195 Dower NA, Stang SL, Bottorff DA, Ebinu JO, Dickie P, Ostergaard HL, Stone JC (2000)
1196 RasGRP is essential for mouse thymocyte differentiation and TCR signaling. Nat Immunol
1197 1:317–321.

1198 Duan X, Qiao M, Bei F, Kim I-J, He Z, Sanes JR (2015) Subtype-Specific Regeneration of
1199 Retinal Ganglion Cells following Axotomy: Effects of Osteopontin and mTOR Signaling.
1200 Neuron 85:1244–1256.

1201 Dumitrescu ON, Pucci FG, Wong KY, Berson DM (2009) Ectopic retinal ON bipolar cell
1202 synapses in the OFF inner plexiform layer: Contacts with dopaminergic amacrine cells and
1203 melanopsin ganglion cells. Journal of Comparative Neurology 517:226–244.

1204 Ebinu JO, Bottorff DA, Chan EY, Stang SL, Dunn RJ, Stone JC (1998) RasGRP, a Ras guanyl
1205 nucleotide- releasing protein with calcium- and diacylglycerol-binding motifs. Science
1206 280:1082–1086.

1207 Ecker JL, Dumitrescu ON, Wong KY, Alam NM, Chen S-K, LeGates T, Renna JM, Prusky GT,
1208 Berson DM, Hattar S (2010) Melanopsin-Expressing Retinal Ganglion-Cell Photoreceptors:
1209 Cellular Diversity and Role in Pattern Vision. Neuron 67:49–60.

1210 Eide EJ, Woolf MF, Kang H, Woolf P, Hurst W, Camacho F, Vielhaber EL, Giovanni A, Virshup
1211 DM (2005) Control of mammalian circadian rhythm by CKIepsilon-regulated proteasome-
1212 mediated PER2 degradation. Mol Cell Biol 25:2795–2807.

1213 Emanuel AJ, Do MTH (2015) Melanopsin Tristability for Sustained and Broadband
1214 Phototransduction. Neuron 85:1043–1055.

1215 Emanuel AJ, Kapur K, Do MTH (2017) Biophysical Variation within the M1 Type of Ganglion
1216 Cell Photoreceptor. Cell Rep 21:1048–1062.

1217 Estevez ME, Fogerson PM, Ilardi MC, Borghuis BG, Chan E, Weng S, Auferkorte ON, Demb
1218 JB, Berson DM (2012) Form and function of the M4 cell, an intrinsically photosensitive
1219 retinal ganglion cell type contributing to geniculocortical vision. J Neurosci 32:13608–13620.

1220 Fernandez DC, Chang Y-T, Hattar S, Chen S-K (2016) Architecture of retinal projections to the
1221 central circadian pacemaker. Proc Natl Acad Sci USA 113:6047–6052.

1222 Fink M, Lesage F, Duprat F, Heurteaux C, Reyes R, Fosset M, Lazdunski M (1998) A neuronal
1223 two P domain K+ channel stimulated by arachidonic acid and polyunsaturated fatty acids.
1224 EMBO J 17:3297–3308.

1225 Fornaro M, Raimondo S, Lee JM, Giuseppina Giacobini-Robecchi M (2007) Neuron-specific Hu
1226 proteins sub-cellular localization in primary sensory neurons. Annals of Anatomy -
1227 Anatomischer Anzeiger 189:223–228.

1228 Frings S, Brüll N, Dzeja C, Angele A, Hagen V, Kaupp UB, Baumann A (1998) Characterization
1229 of ether-à-go-go channels present in photoreceptors reveals similarity to IKx, a K+ current in
1230 rod inner segments. J Gen Physiol 111:583–599.

1231 Gorentla BK, Wan C-K, Zhong X-P (2011) Negative regulation of mTOR activation by
1232 diacylglycerol kinases. Blood 117:4022–4031.

1233 Graham DM, Wong KY, Shapiro P, Frederick C, Pattabiraman K, Berson DM (2008) Melanopsin
1234 Ganglion Cells Use a Membrane-Associated Rhabdomeric Phototransduction Cascade.
1235 Journal of Neurophysiology 99:2522–2532.

1236 Haeryfar SMM, Hoskin DW (2004) Thy-1: More than a Mouse Pan-T Cell Marker. The Journal of
1237 Immunology 173:3581–3588.

1238 Hannibal J, Hindersson P, Østergaard J, Georg B, Heegaard S, Larsen PJ, Fahrenkrug J (2004)
1239 Melanopsin Is Expressed in PACAP-Containing Retinal Ganglion Cells of the Human
1240 Retinohypothalamic Tract. Invest Ophthalmol Vis Sci 45:4202–4209.

1241 Hartwick ATE, Bramley JR, Yu J, Stevens KT, Allen CN, Baldridge WH, Sollars PJ, Pickard GE
1242 (2007) Light-evoked calcium responses of isolated melanopsin-expressing retinal ganglion
1243 cells. J Neurosci 27:13468–13480.

1244 Hattar S, Kumar M, Park A, Tong P, Tung J, Yau K-W, Berson DM (2006) Central projections of
1245 melanopsin-expressing retinal ganglion cells in the mouse. J Comp Neurol 497:326–349.

1246 Heiman M, Schaefer A, Gong S, Peterson JD, Day M, Ramsey KE, Suárez-Fariñas M, Schwarz
1247 C, Stephan DA, Surmeier DJ, Greengard P, Heintz N (2008) A Translational Profiling
1248 Approach for the Molecular Characterization of CNS Cell Types. Cell 135:738–748.

1249 Hinman MN, Lou H (2008) Diverse molecular functions of Hu proteins. Cell Mol Life Sci
1250 65:3168–3181.

1251 Hoshi H, Liu W-L, Massey SC, Mills SL (2009) ON inputs to the OFF layer: bipolar cells that
1252 break the stratification rules of the retina. J Neurosci 29:8875–8883.

1253 Hu C, Hill DD, Wong KY (2013) Intrinsic physiological properties of the five types of mouse
1254 ganglion-cell photoreceptors. Journal of Neurophysiology 109:1876–1889.

1255 Hughes S, Hankins MW, Foster RG, Peirson SN (2012) Melanopsin phototransduction: slowly
1256 emerging from the dark. Prog Brain Res 199:19–40.

1257 Hughes S, Jagannath A, Hickey D, Gatti S, Wood M, Peirson SN, Foster RG, Hankins MW
1258 (2015) Using siRNA to define functional interactions between melanopsin and multiple G
1259 Protein partners. Cell Mol Life Sci 72:165–179.

1260 Jain V, Ravindran E, Dhingra NK (2012) Differential expression of Brn3 transcription factors in
1261 intrinsically photosensitive retinal ganglion cells in mouse. Journal of Comparative
1262 Neurology 520:742–755.

1263 Jeon C-J, Strettoi E, Masland RH (1998) The Major Cell Populations of the Mouse Retina. J
1264 Neurosci 18:8936–8946.

1265 Ji M, Zhao W-J, Dong L-D, Miao Y, Yang X-L, Sun X-H, Wang Z (2011) RGS2 and RGS4
1266 modulate melatonin-induced potentiation of glycine currents in rat retinal ganglion cells.
1267 Brain Research 1411:1–8.

1268 Jiang Z, Yue WWS, Chen L, Sheng Y, Yau KW (2018) Cyclic-Nucleotide- and HCN-Channel-
1269 Mediated Phototransduction in Intrinsically Photosensitive Retinal Ganglion Cells. Cell.
1270 175(3):652-664.e12.

1271 Kim I-J, Zhang Y, Meister M, Sanes JR (2010) Laminar restriction of retinal ganglion cell
1272 dendrites and axons: subtype-specific developmental patterns revealed with transgenic
1273 markers. J Neurosci 30:1452–1462.

1274 Koussounadis A, Langdon SP, Um IH, Harrison DJ, Smith VA (2015) Relationship between
1275 differentially expressed mRNA and mRNA-protein correlations in a xenograft model system.
1276 Sci Rep 5:10775.

1277 Li JY, Schmidt TM. Divergent projection patterns of M1 ipRGC subtypes (2018) J Comp Neurol.
1278 526(13):2010-2018.

1279 Li S, Yang C, Zhang L, Gao X, Wang X, Liu W, Wang Y, Jiang S, Wong YH, Zhang Y, Liu K
1280 (2016) Promoting axon regeneration in the adult CNS by modulation of the
1281 melanopsin/GPCR signaling. Proc Natl Acad Sci USA 113:1937–1942.

1282 Li S-Y, Yau S-Y, Chen B-Y, Tay DK, Lee VWH, Pu M-L, Chan HHL, So K-F (2008) Enhanced
1283 Survival of Melanopsin-expressing Retinal Ganglion Cells After Injury is Associated with the
1284 PI3 K/Akt Pathway. Cell Mol Neurobiol 28:1095–1107.

1285 Lin JC, Ho W-H, Gurney A, Rosenthal A (2003) The netrin-G1 ligand NGL-1 promotes the
1286 outgrowth of thalamocortical axons. Nature Neuroscience 6:1270–1276.

1287 Lin Z, Liu J, Ding H, Xu F, Liu H (2018) Structural basis of SALM5-induced PTPδ dimerization
1288 for synaptic differentiation. Nature Communications 9:268.

1289 Lipina TV, Prasad T, Yokomaku D, Luo L, Connor SA, Kawabe H, Wang YT, Brose N, Roder
1290 JC, Craig AM (2016) Cognitive Deficits in Calsyntenin-2-deficient Mice Associated with
1291 Reduced GABAergic Transmission. Neuropsychopharmacology 41:802–810.

1292 Lobo MK, Karsten SL, Gray M, Geschwind DH, Yang XW (2006) FACS-array profiling of striatal
1293 projection neuron subtypes in juvenile and adult mouse brains. Nature Neuroscience 9:443–
1294 452.

1295 Macosko EZ, Basu A, Satija R, Nemesh J, Shekhar K, Goldman M, Tirosh I, Bialas AR,
1296 Kamitaki N, Martersteck EM, Trombetta JJ, Weitz DA, Sanes JR, Shalek AK, Regev A,
1297 McCarroll SA (2015) Highly Parallel Genome-wide Expression Profiling of Individual Cells
1298 Using Nanoliter Droplets. Cell 161:1202–1214.

1299 Mao C-A, Kiyama T, Pan P, Furuta Y, Hadjantonakis A-K, Klein WH (2008) Eomesodermin, a
1300 target gene of Pou4f2, is required for retinal ganglion cell and optic nerve development in
1301 the mouse. Development 135:271–280.

1302 Mao C-A, Li H, Zhang Z, Kiyama T, Panda S, Hattar S, Ribelayga CP, Mills SL, Wang SW
1303 (2014) T-box transcription regulator Tbr2 is essential for the formation and maintenance of
1304 Opn4/melanopsin-expressing intrinsically photosensitive retinal ganglion cells. J Neurosci
1305 34:13083–13095.

1306 Mao H, Zhao Q, Daigle M, Ghahremani MH, Chidiac P, Albert PR (2004) RGS17/RGSZ2, a
1307 novel regulator of Gi/o, Gz, and Gq signaling. J Biol Chem 279:26314–26322.

1308 Martin S, Lino de Oliveira C, Mello de Queiroz F, Pardo LA, Stühmer W, Del Bel E (2008) Eag1
1309 potassium channel immunohistochemistry in the CNS of adult rat and selected regions of
1310 human brain. Neuroscience 155:833–844.

1311 Matsuoka RL, Nguyen-Ba-Charvet KT, Parray A, Badea TC, Chédotal A, Kolodkin AL (2011)
1312 Transmembrane semaphorin signalling controls laminar stratification in the mammalian
1313 retina. Nature 470:259–263.

1314 Matsushima D, Heavner W, Pevny LH (2011) Combinatorial regulation of optic cup progenitor
1315 cell fate by SOX2 and PAX6. Development 138:443–454.

1316 Missler M, Hammer RE, Südhof TC (1998) Neurexophilin binding to alpha-neurexins. A single
1317 LNS domain functions as an independently folding ligand-binding unit. J Biol Chem
1318 273:34716–34723.

1319 Moises HC, Rusin KI, Macdonald RL (1994) Mu- and kappa-opioid receptors selectively reduce
1320 the same transient components of high-threshold calcium current in rat dorsal root ganglion
1321 sensory neurons. J Neurosci 14:5903–5916.

1322 Morrow EM, Belliveau MJ, Cepko CL (1998) Two Phases of Rod Photoreceptor Differentiation
1323 during Rat Retinal Development. J Neurosci 18:3738–3748.

1324 Morse AM, Carballo V, Baldwin DA, Taylor CG, McIntyre LM (2010) Comparison between
1325 NuGEN's WT-Ovation Pico and one-direct amplification systems. J Biomol Tech 21:141–
1326 147.

1327 Mure LS, Hatori M, Ruda K, Benegiamo G, Demas J, Panda S (2018) Sustained Melanopsin
1328 Photoresponse Is Supported by Specific Roles of β-Arrestin 1 and 2 in Deactivation and
1329 Regeneration of Photopigment. Cell Rep. 25(9):2497-2509.e4.

1330 Naiche LA, Harrelson Z, Kelly RG, Papaioannou VE (2005) T-box genes in vertebrate
1331 development. Annu Rev Genet 39:219–239.

1332 Novak A, Guo C, Yang W, Nagy A, Lobe CG (2000) Z/EG, a double reporter mouse line that
1333 expresses enhanced green fluorescent protein upon Cre-mediated excision. Genesis.

1334 Oancea E, Meyer T (1998) Protein kinase C as a molecular machine for decoding calcium and
1335 diacylglycerol signals. Cell 95:307–318.

1336 Pack W, Hill DD, Wong KY (2015) Melatonin modulates M4-type ganglion-cell photoreceptors.
1337 Neuroscience 303:178–188.

1338 Pederick DT, Homan CC, Jaehne EJ, Piltz SG, Haines BP, Baune BT, Jolly LA, Hughes JN,
1339 Gecz J, Thomas PQ (2016) Pcdh19 Loss-of-Function Increases Neuronal Migration In Vitro
1340 but is Dispensable for Brain Development in Mice. Sci Rep 6:26765.

1341 Peirson SN, Oster H, Jones SL, Leitges M, Hankins MW, Foster RG (2007) Microarray Analysis
1342 and Functional Genomics Identify Novel Components of Melanopsin Signaling. Current
1343 Biology 17:1363–1372.

1344 Pettem KL, Yokomaku D, Takahashi H, Ge Y, Craig AM (2013) Interaction between autism-
1345 linked MDGAs and neuroligins suppresses inhibitory synapse development. J Cell Biol
1346 200:321–336.

1347 Pierret P, Dunn RJ, Djordjevic B, Stone JC, Richardson PM (2000) Distribution of ras guanyl
1348 releasing protein (RasGRP) mRNA in the adult rat central nervous system. J Neurocytol
1349 29:485–497.

1350 Pocock R, Mione M, Hussain S, Maxwell S, Pontecorvi M, Aslam S, Gerrelli D, Sowden JC,
1351 Woollard A (2008) Neuronal function of Tbx20 conserved from nematodes to vertebrates.
1352 Developmental Biology 317:671–685.

1353 Puente LG, Stone JC, Ostergaard HL (2000) Evidence for protein kinase C-dependent and -
1354 independent activation of mitogen-activated protein kinase in T cells: potential role of
1355 additional diacylglycerol binding proteins. The Journal of Immunology 165:6865–6871.

1356 Quail MA, Kozarewa I, Smith F, Scally A, Stephens PJ, Durbin R, Swerdlow H, Turner DJ
1357 (2008) A large genome center's improvements to the Illumina sequencing system. Nat
1358 Methods 5:1005–1010.

1359 Quattrochi LE, Stabio ME, Kim I, Ilardi MC, Michelle Fogerson P, Leyrer ML, Berson DM (2019)
1360 The M6 cell: A small-field bistratified photosensitive retinal ganglion cell. J Comp Neurol.
1361 527(1):297-311.

1362 Reifler AN, Chervenak AP, Dolikian ME, Benenati BA, Li BY, Wachter RD, Lynch AM,
1363 Demertzis ZD, Meyers BS, Abufarha FS, Jaeckel ER, Flannery MP, Wong KY (2015) All
1364 Spiking, Sustained ON Displaced Amacrine Cells Receive Gap-Junction Input from
1365 Melanopsin Ganglion Cells. Current Biology 25:2763–2773.

1366 Renna JM, Weng S, Berson DM (2011) Light acts through melanopsin to alter retinal waves and
1367 segregation of retinogeniculate afferents. Nature Neuroscience 14:827–829.

1368 Rheaume BA, Jereen A, Bolisetty M, Sajid MS, Yang Y, Renna K, Sun L, Robson P,
1369 Trakhtenberg EF (2018) Single cell transcriptome profiling of retinal ganglion cells identifies
1370 cellular subtypes. Nat Commun. 2018 Jul 17;9(1):2759.

1371 Rodriguez AR, Sevilla Müller LP, Brecha NC (2014) The RNA binding protein RBPMS is a
1372 selective marker of ganglion cells in the mammalian retina. Journal of Comparative
1373 Neurology 522:1411–1443.

1374 Rousso DL, Qiao M, Kagan RD, Yamagata M, Palmiter RD, Sanes JR (2016) Two Pairs of ON
1375 and OFF Retinal Ganglion Cells Are Defined by Intersectional Patterns of Transcription
1376 Factor Expression. Cell Rep 15:1930–1944.

1377 Sabbah S, Berg D, Papendorp C, Briggman KL, Berson DM (2017) A Cre Mouse Line for
1378 Probing Irradiance- and Direction-Encoding Retinal Networks. eNeuro 4:ENEURO.0065–
1379 17.2017.

1380 Sakabe NJ, Aneas I, Shen T, Shokri L, Park S-Y, Bulyk ML, Evans SM, Nobrega MA (2012)
1381 Dual transcriptional activator and repressor roles of TBX20 regulate adult cardiac structure
1382 and function. Hum Mol Genet 21:2194–2204.

1383 Sand A, Schmidt TM, Kofuji P (2012) Diverse types of ganglion cell photoreceptors in the
1384 mammalian retina. Progress in Retinal and Eye Research 31:287–302.

1385 Sanes JR, Masland RH (2015) The Types of Retinal Ganglion Cells: Current Status and
1386 Implications for Neuronal Classification. http://dxdoiorg/101146/annurev-neuro-071714-
1387 034120 38:221–246.

1388 Schmidt TM, Do MTH, Dacey D, Lucas R, Hattar S, Matynia A (2011) Melanopsin-positive
1389 intrinsically photosensitive retinal ganglion cells: from form to function. J Neurosci
1390 31:16094–16101.

1391 Schmidt TM, Taniguchi K, Kofuji P (2008) Intrinsic and Extrinsic Light Responses in
1392 Melanopsin-Expressing Ganglion Cells During Mouse Development. Journal of
1393 Neurophysiology 100:371–384.

1394 Sengupta A, Baba K, Mazzoni F, Pozdeyev NV, Strettoi E, Iuvone PM, Tosini G (2011)
1395 Localization of melatonin receptor 1 in mouse retina and its role in the circadian regulation
1396 of the electroretinogram and dopamine levels. Yamazaki S, ed. PLoS ONE 6:e24483.

1397 Shekhar K, Lapan SW, Whitney IE, Tran NM, Macosko EZ, Kowalczyk M, Adiconis X, Levin JZ,
1398 Nemesh J, Goldman M, McCarroll SA, Cepko CL, Regev A, Sanes JR (2016)
1399 Comprehensive Classification of Retinal Bipolar Neurons by Single-Cell Transcriptomics.
1400 Cell 166:1308–1323.e1330.

1401 Shen T, Aneas I, Sakabe N, Dirschinger RJ, Wang G, Smemo S, Westlund JM, Cheng H,
1402 Dalton N, Gu Y, Boogerd CJ, Cai C-L, Peterson K, Chen J, Nobrega MA, Evans SM (2011)
1403 Tbx20 regulates a genetic program essential to adult mouse cardiomyocyte function. J Clin
1404 Invest 121:4640–4654.

1405 Sheng W-L, Chen W-Y, Yang X-L, Zhong Y-M, Weng S-J (2015) Co-expression of two subtypes
1406 of melatonin receptor on rat M1-type intrinsically photosensitive retinal ganglion cells.
1407 Barnes S, ed. PLoS ONE 10:e0117967.

1408 Shulga YV, Topham MK, Epand RM (2011) Regulation and Functions of Diacylglycerol Kinases.
1409 Chemical Reviews 111:6186–6208.

1410 Siegert S, Cabuy E, Scherf BG, Kohler H, Panda S, Le Y-Z, Fehling HJ, Gaidatzis D, Stadler
1411 MB, Roska B (2012) Transcriptional code and disease map for adult retinal cell types.
1412 Nature Neuroscience 15:487–495.

1413 Sonoda T, Lee SK, Birnbaumer L, Schmidt TM (2018) Melanopsin Phototransduction Is
1414 Repurposed by ipRGC Subtypes to Shape the Function of Distinct Visual Circuits. Neuron.
1415 99(4):754-767.e4.

1416 Soto I, Oglesby E, Buckingham BP, Son JL, Roberson EDO, Steele MR, Inman DM, Vetter ML,
1417 Horner PJ, Marsh-Armstrong N (2008) Retinal Ganglion Cells Downregulate Gene
1418 Expression and Lose Their Axons within the Optic Nerve Head in a Mouse Glaucoma
1419 Model. J Neurosci 28:548–561.

1420 Stabio ME, Sabbah S, Quattrochi LE, Ilardi MC, Fogerson PM, Leyrer ML, Kim MT, Kim I, Schiel
1421 M, Renna JM, Briggman KL, Berson DM (2018) The M5 Cell: A Color-Opponent Intrinsically
1422 Photosensitive Retinal Ganglion Cell. Neuron 97:251.

1423 Star EN, Zhu M, Shi Z, Liu H, Pashmforoush M, Sauve Y, Bruneau BG, Chow RL (2012)
1424 Regulation of retinal interneuron subtype identity by the Iroquois homeobox gene Irx6.
1425 Development 139:4644–4655.

1426 Stennard FA, Costa MW, Elliott DA, Rankin S, Haast SJP, Lai D, McDonald LPA, Niederreither
1427 K, Dolle P, Bruneau BG, Zorn AM, Harvey RP (2003) Cardiac T-box factor Tbx20 directly
1428 interacts with Nkx2-5, GATA4, and GATA5 in regulation of gene expression in the
1429 developing heart. Developmental Biology 262:206–224.

1430 Sweeney NT, Tierney H, Feldheim DA (2014) Tbr2 is required to generate a neural circuit
1431 mediating the pupillary light reflex. J Neurosci 34:5447–5453.

1432 Takeuchi JK, Mileikovskaia M, Koshiba-Takeuchi K, Heidt AB, Mori AD, Arruda EP,
1433 Gertsenstein M, Georges R, Davidson L, Mo R, Hui C-C, Henkelman RM, Nemer M, Black
1434 BL, Nagy A, Bruneau BG (2005) Tbx20 dose-dependently regulates transcription factor
1435 networks required for mouse heart and motoneuron development. Development 132:2463–
1436 2474.

1437 Tariq MA, Kim HJ, Jejelowo O, Pourmand N (2011) Whole-transcriptome RNAseq analysis from
1438 minute amount of total RNA. Nucleic Acids Res 39:e120–e120.

1439 Thorvaldsdóttir H, Robinson JT (2013) Integrative Genomics Viewer (IGV): high-performance
1440 genomics data visualization and exploration. Briefings in ….

1441 Toki S, Kawasaki H, Tashiro N, Housman DE, Graybiel AM (2001) Guanine nucleotide
1442 exchange factors CalDAG-GEFI and CalDAG-GEFII are colocalized in striatal projection
1443 neurons. J Comp Neurol 437:398–407.

1444 Topark-Ngarm A, Golonzhka O, Peterson VJ, Barrett B, Martinez B, Crofoot K, Filtz TM, Leid M
1445 (2006) CTIP2 associates with the NuRD complex on the promoter of p57KIP2, a newly
1446 identified CTIP2 target gene. J Biol Chem 281:32272–32283.

1447 Topham MK, Prescott SM (2001) Diacylglycerol kinase zeta regulates Ras activation by a novel
1448 mechanism. J Cell Biol 152:1135–1143.

1449 Trapnell C, Roberts A, Goff L, Pertea G, Kim D, Kelley DR, Pimentel H, Salzberg SL, Rinn JL,
1450 Pachter L (2012) Differential gene and transcript expression analysis of RNA-seq
1451 experiments with TopHat and Cufflinks. Nature Protocols 7:562–578.

1452 Van Hook MJ, Wong KY, Berson DM (2012) Dopaminergic modulation of ganglion-cell
1453 photoreceptors in rat. European Journal of Neuroscience 35:507–518.

1454 Wong KY (2012) A retinal ganglion cell that can signal irradiance continuously for 10 hours. J
1455 Neurosci 32:11478–11485.

1456 Xu J, Xiao N, Xia J (2010) Thrombospondin 1 accelerates synaptogenesis in hippocampal
1457 neurons through neuroligin 1. Nature Neuroscience 13:22–24.

1458 Xue T, Do MTH, Riccio A, Jiang Z, Hsieh J, Wang HC, Merbs SL, Welsbie DS, Yoshioka T,
1459 Weissgerber P, Stolz S, Flockerzi V, Freichel M, Simon MI, Clapham DE, Yau KW (2011)
1460 Melanopsin signalling in mammalian iris and retina. Nature 479:67–73.

1461 Young RW (1985) Cell differentiation in the retina of the mouse. The Anatomical Record
1462 212:199–205.

1463 Zhang M, Xia H, Li X, Wang X, Dong Y, Zhang T, Yu H (2010) C1 domain mediates CalDAGIII
1464 localization to the Golgi. Mol Biol Rep 37:3481–3485.

1465 Zhou H, Yoshioka T, Nathans J (1996) Retina-derived POU-domain factor-1: a complex POU-
1466 domain gene implicated in the development of retinal ganglion and amacrine cells. J
1467 Neurosci 16:2261–2274.

1468

Figure 1.

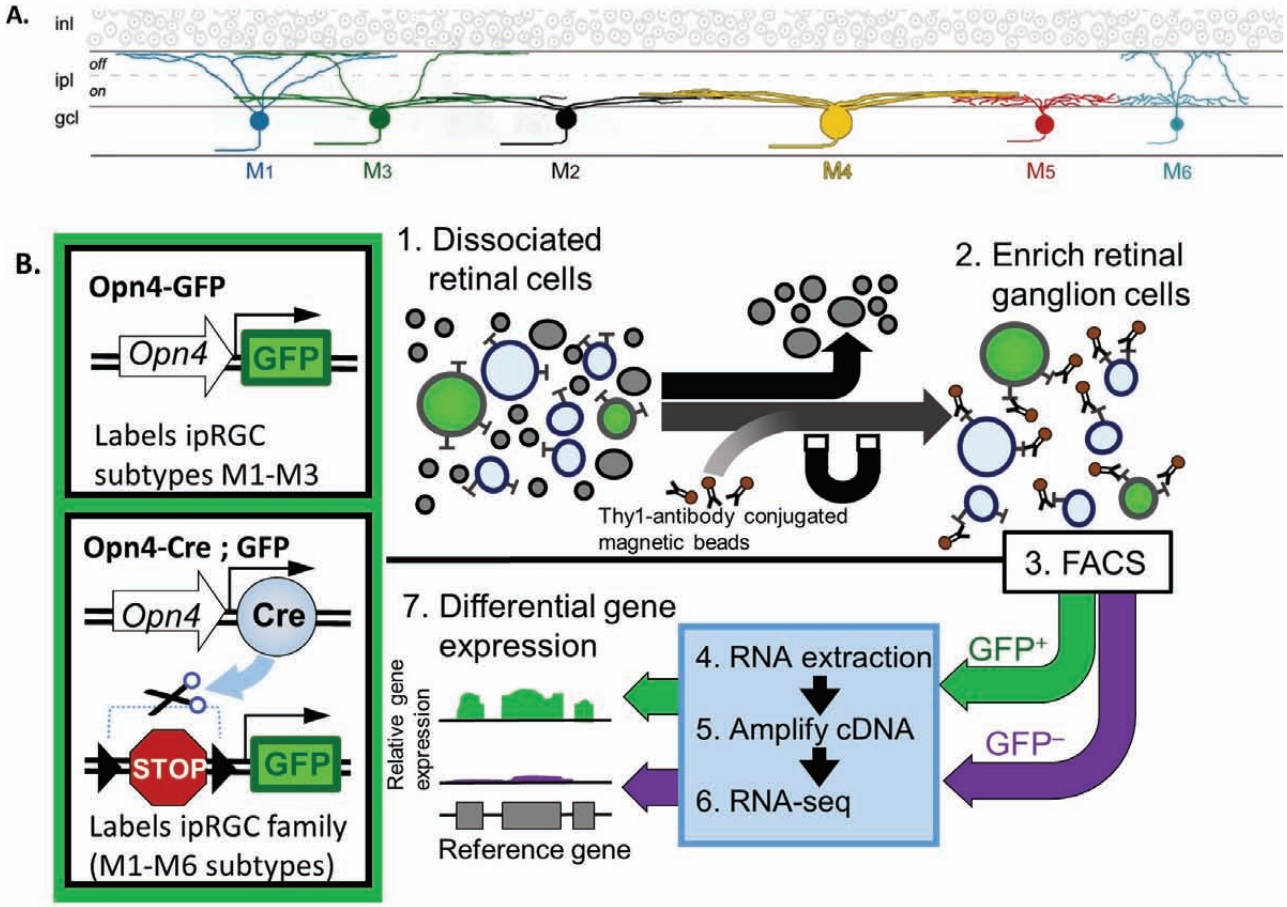

Figure 2.

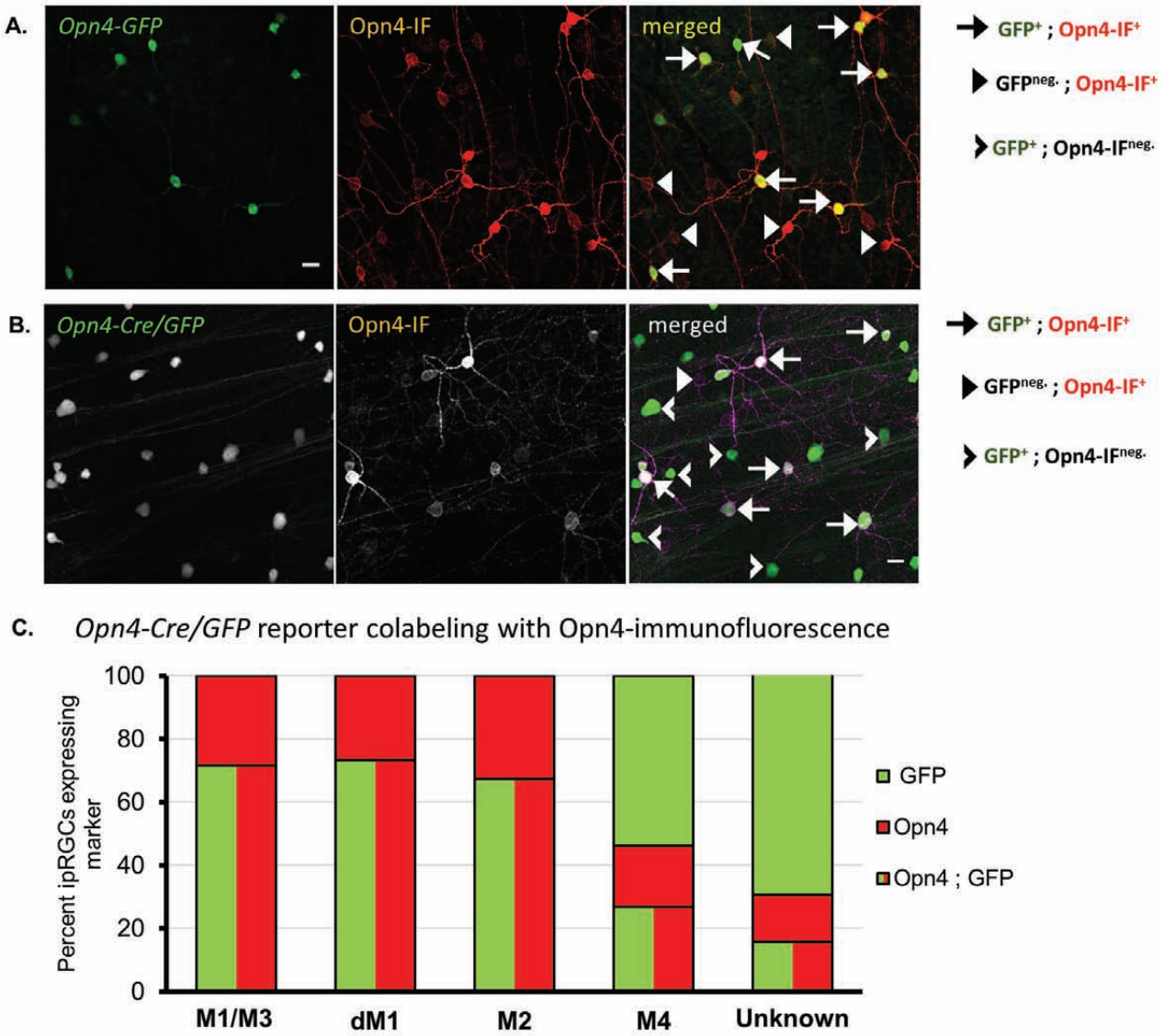

Figure 3.

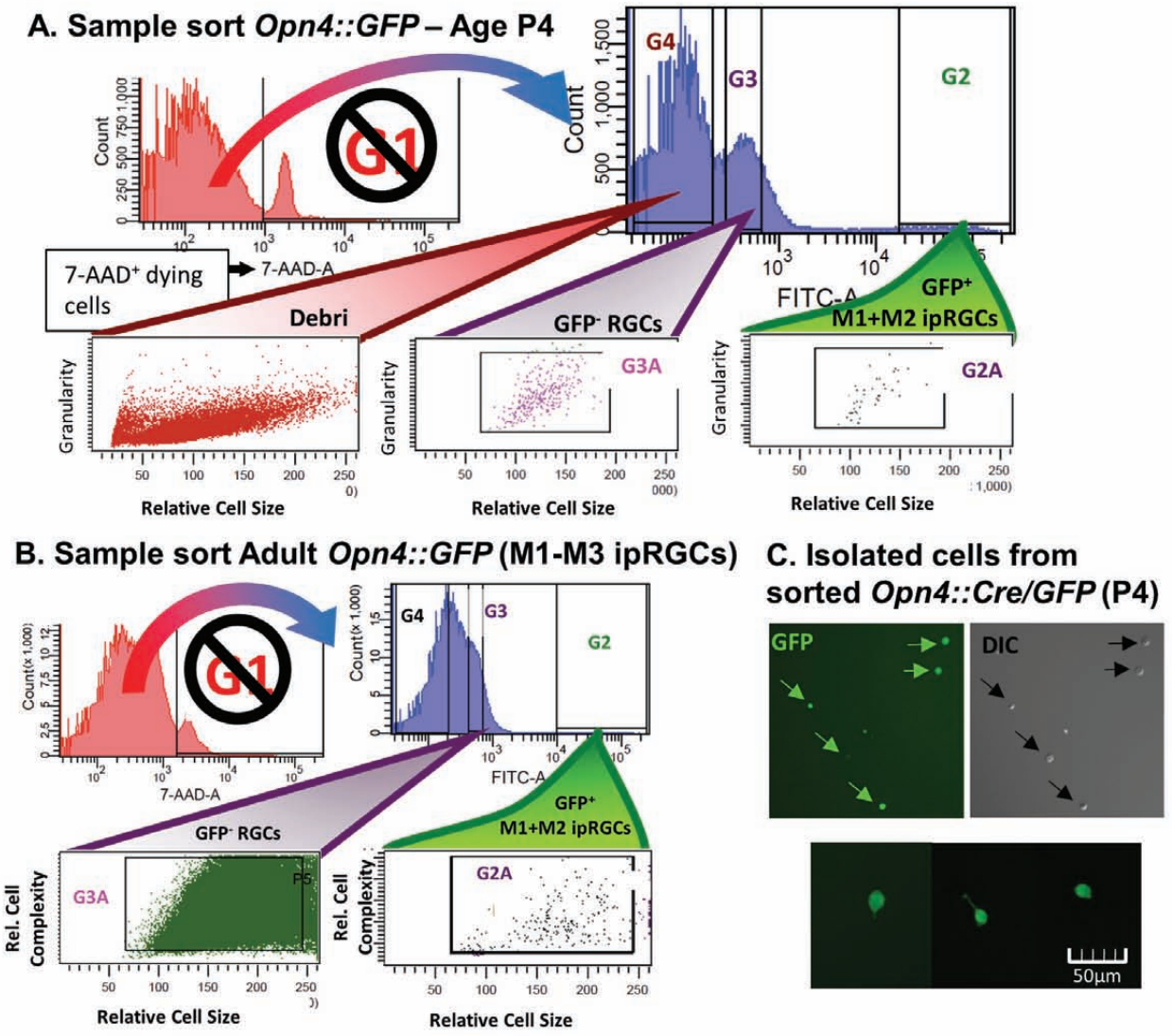

D.

Adult *Opn4-GFP* (M1-M3 ipRGCs)

ipRGCs (GFP+)	reads (millions)	cRGCs (GFP-)	reads (millions)
i4	95.0*	c4	90.9*
i5	44.2*	c5	43.7*
i6	45.6*	c6	49.1*
i7	49.7*	c7	47.3*
i8	10.7	c8	11.3
i9	11.4	c9	22.8

Adult *Opn4-Cre/GFP* (M1-M6 ipRGCs)

ipRGCs (GFP+)	reads (millions)	cRGCs (GFP-)	reads (millions)
i10	109.8*	c10	96.0*
i11	98.6*	c11	110.3*
i12	64.2*	c12	68.9*
i13	21.6	c13	22.0

* concatenated technical replicates

Figure 4.

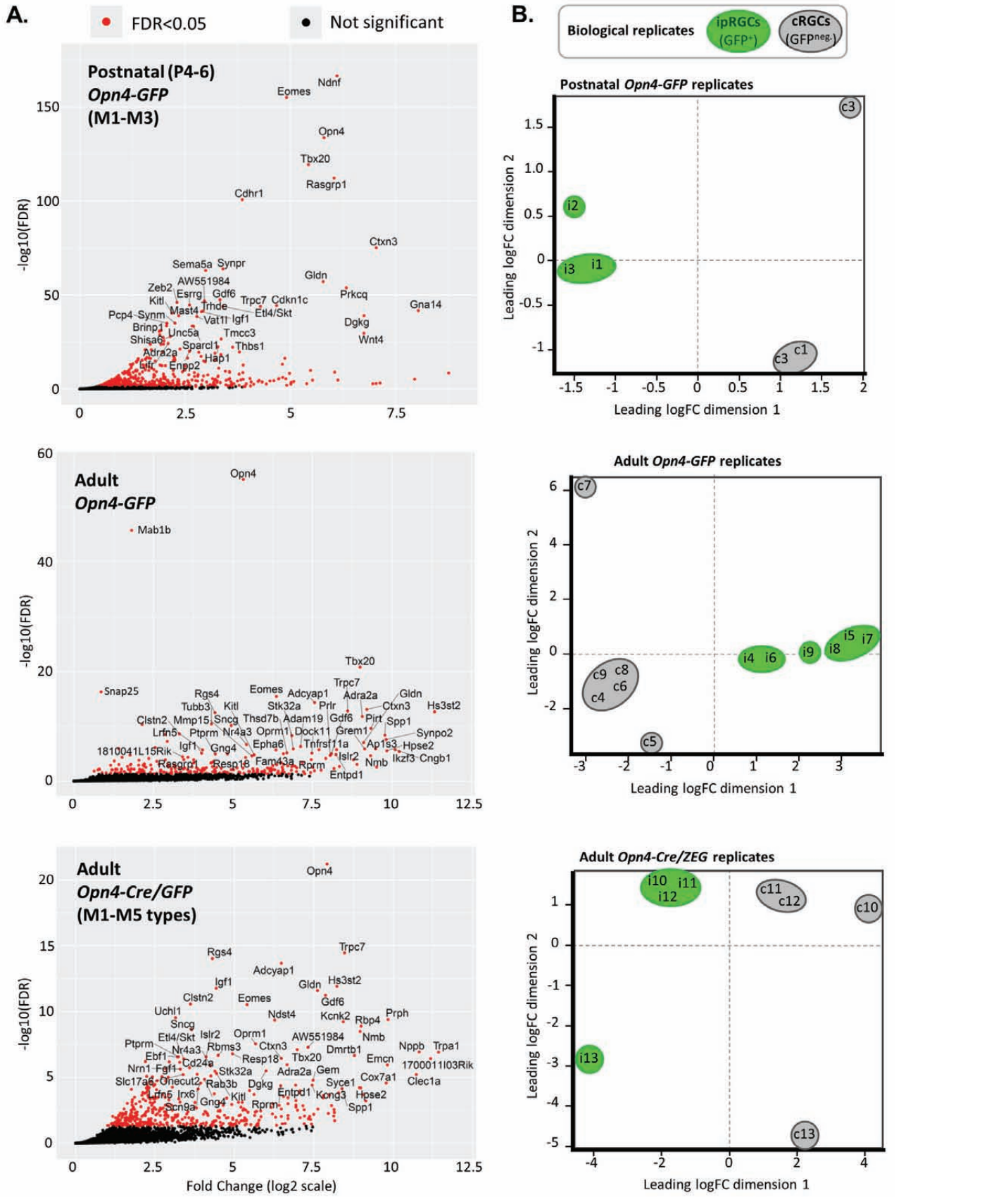

Figure 5

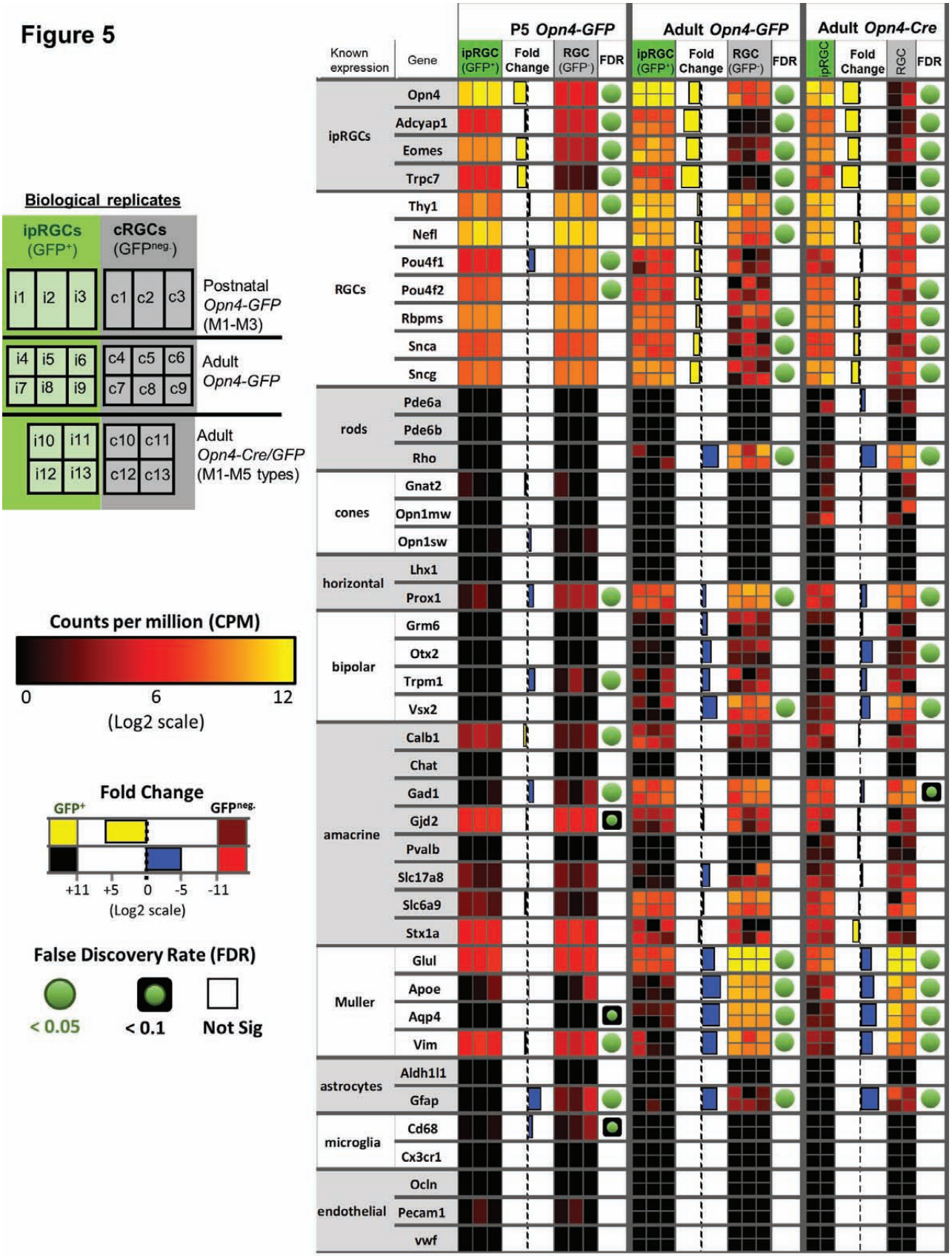

Figure 6

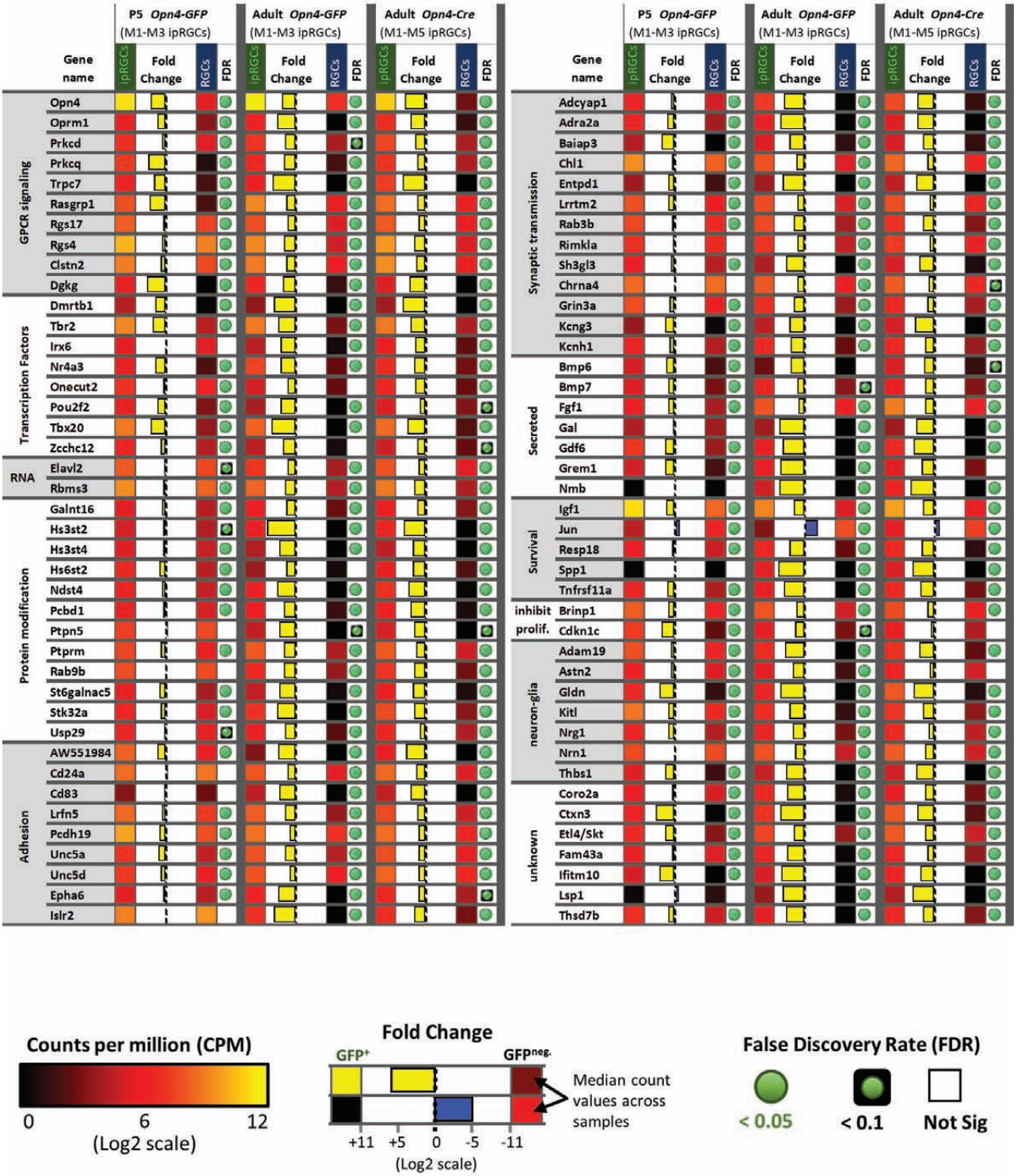

Figure 7

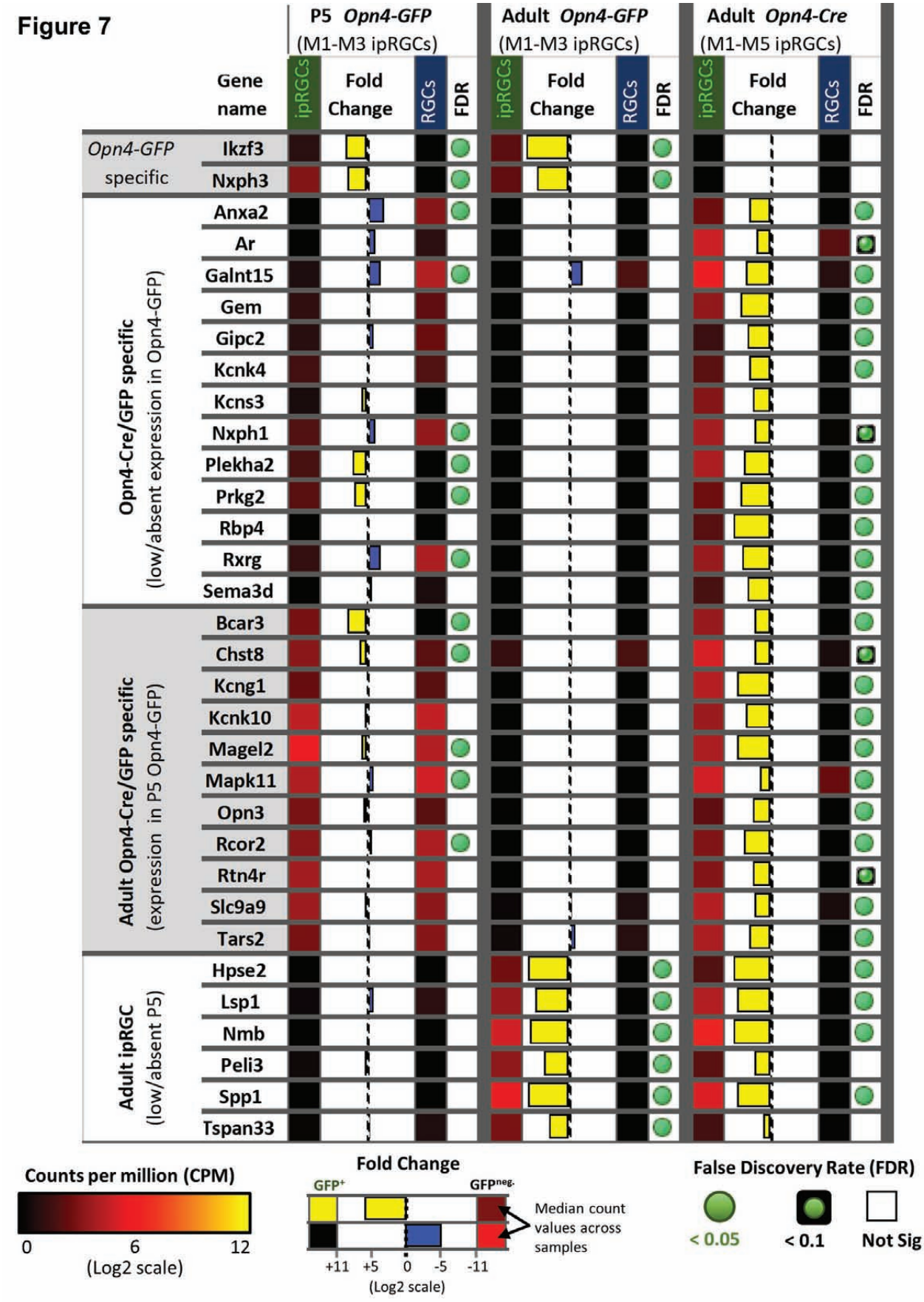

Figure 8

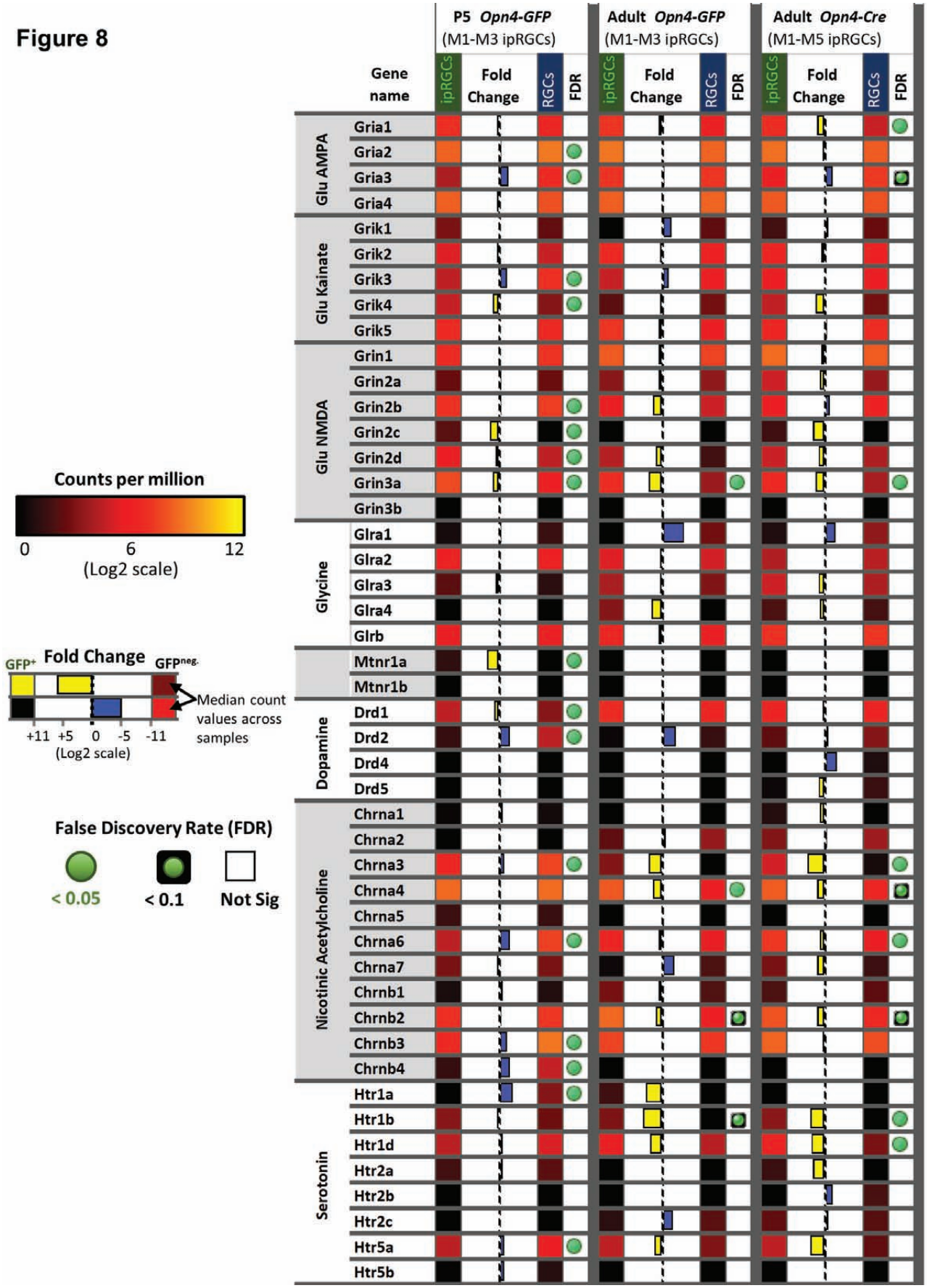

Figure 9

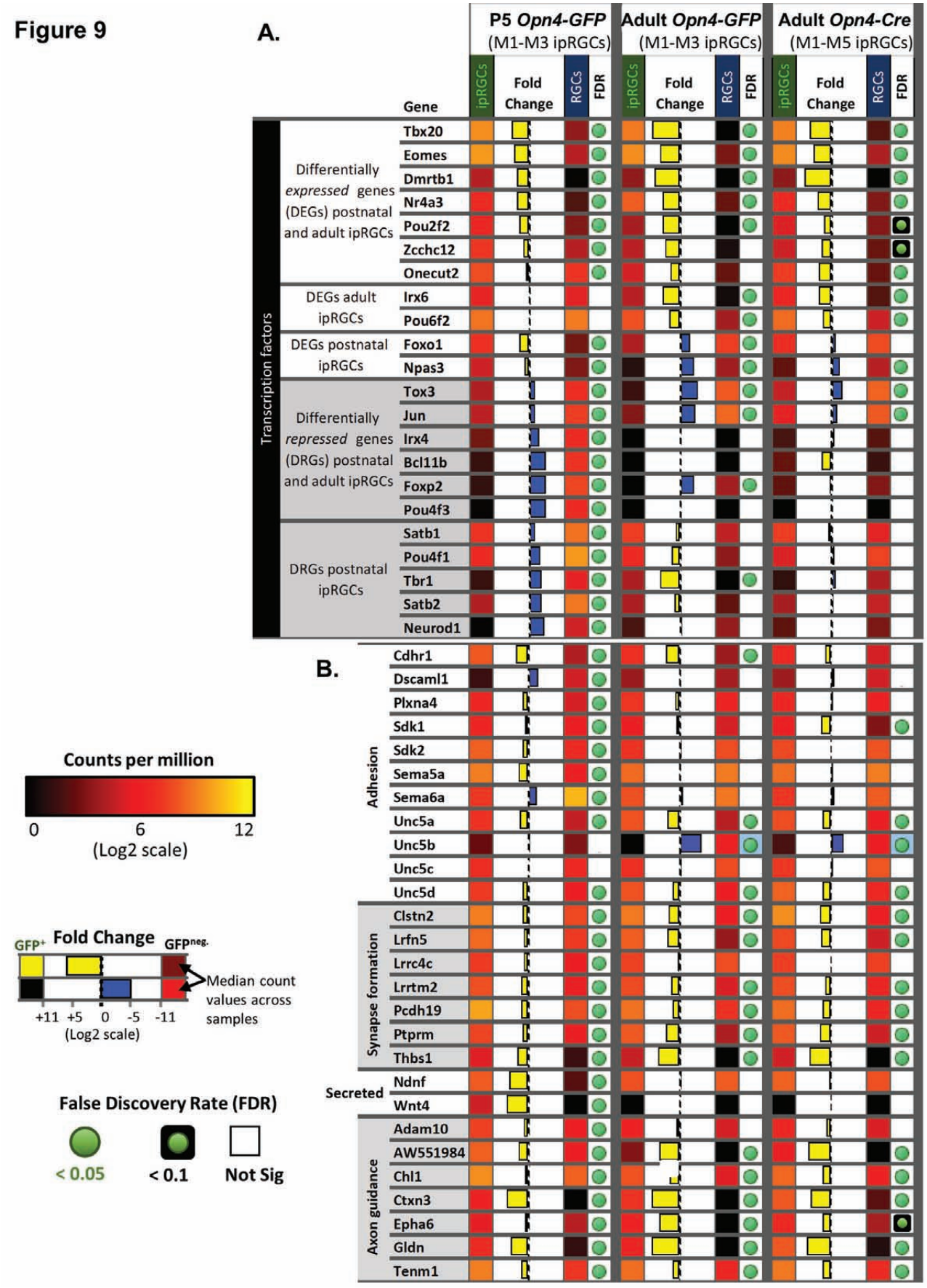

Figure 10.

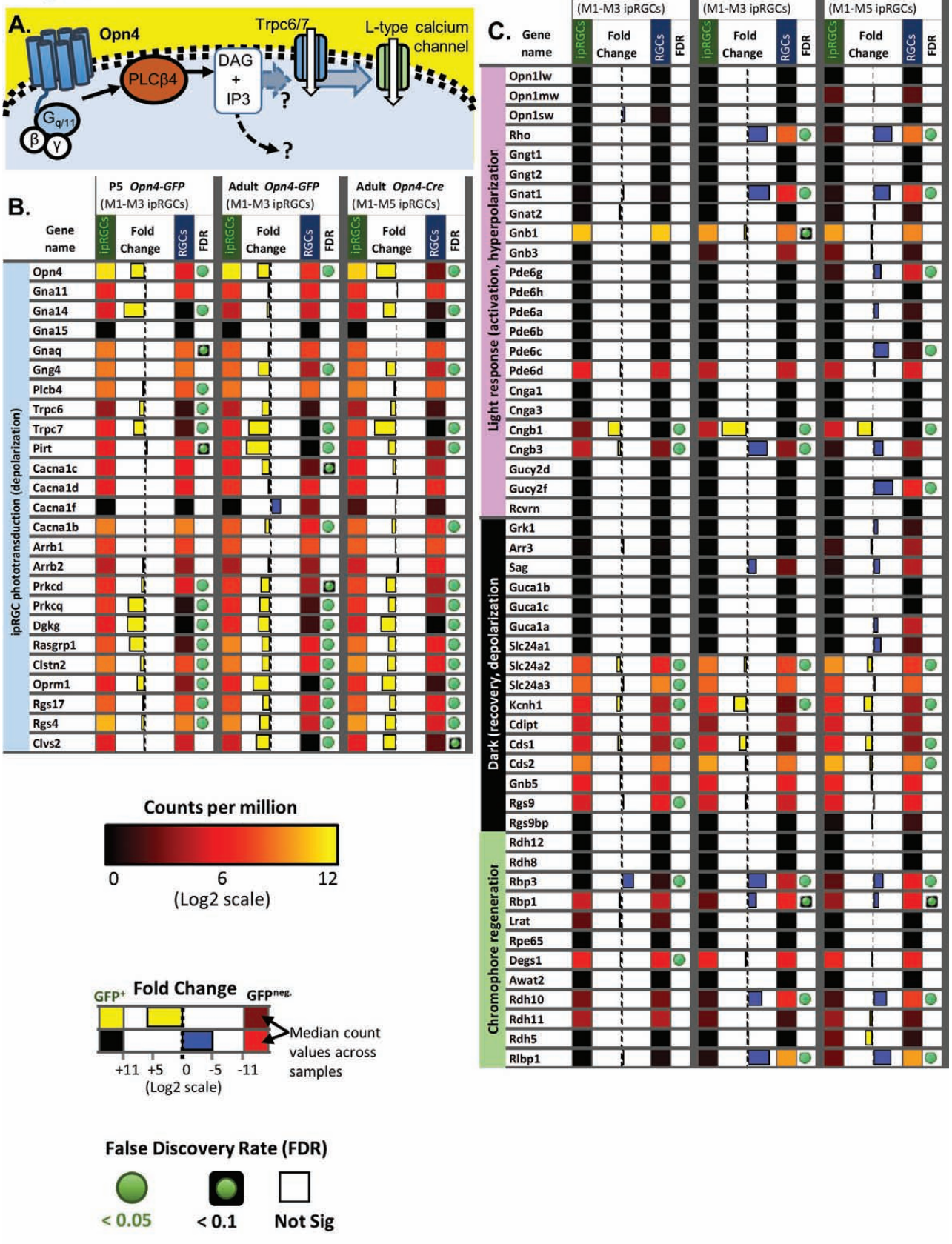

Figure 11.

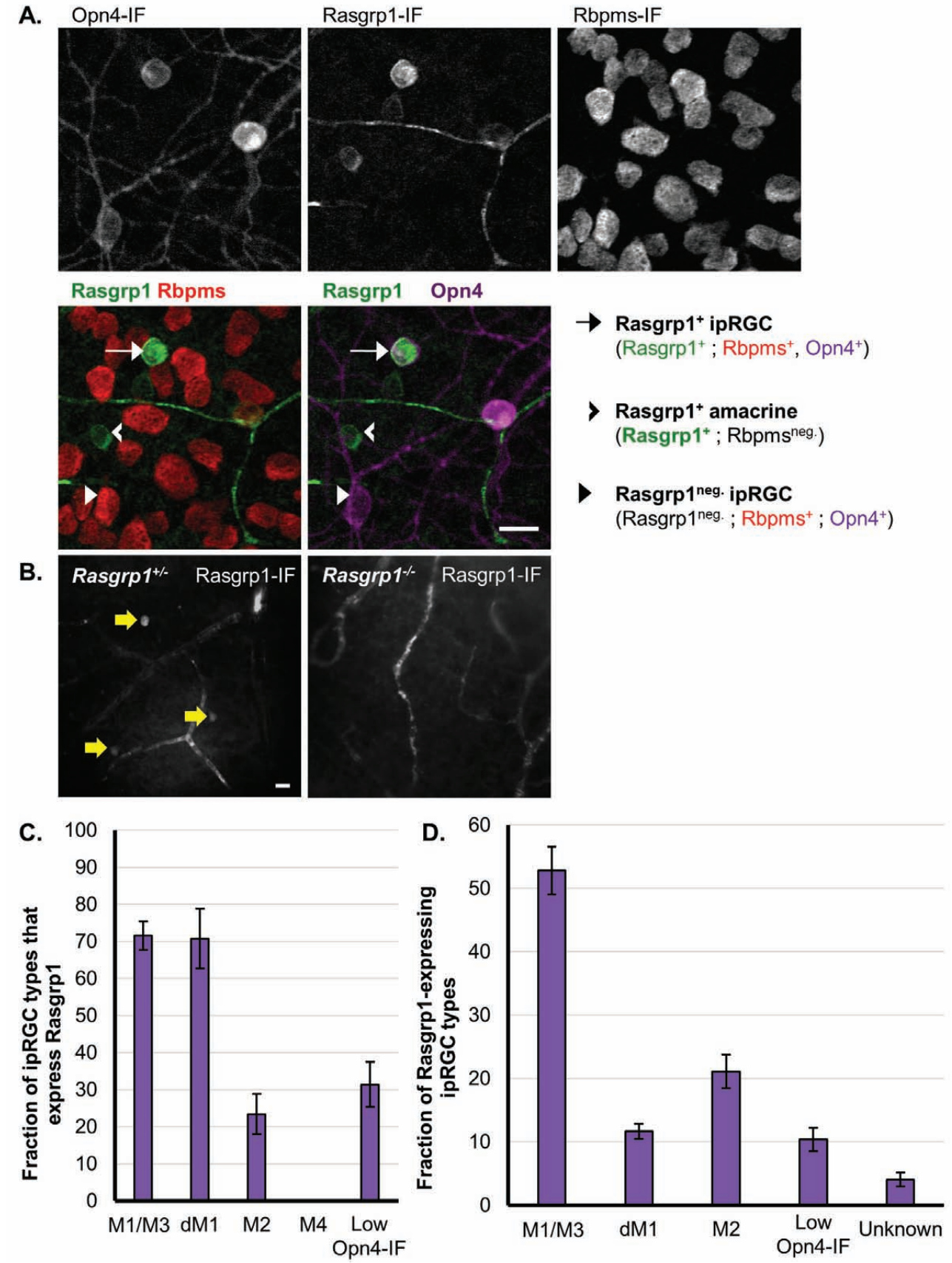

Figure 12.

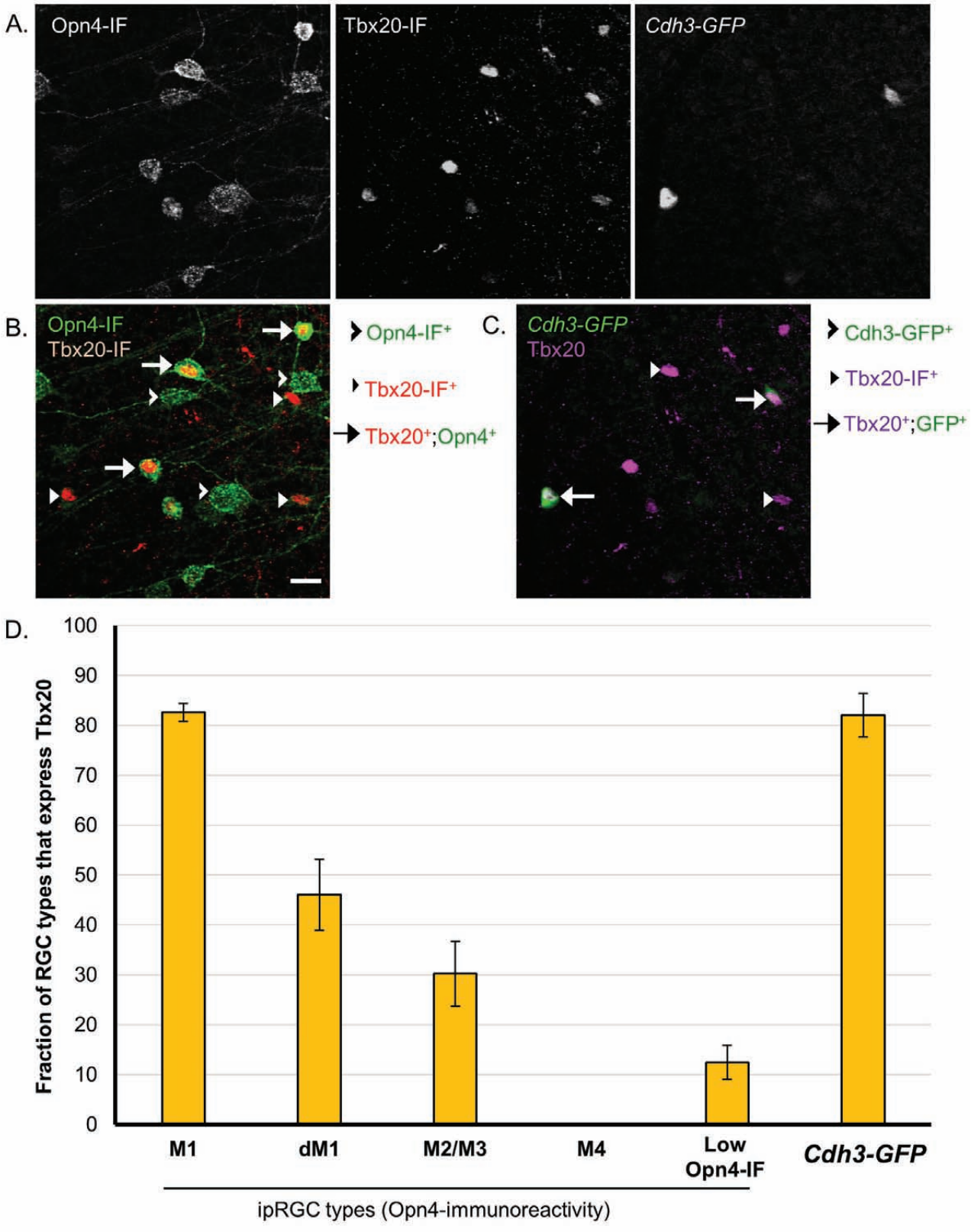

Figure 13

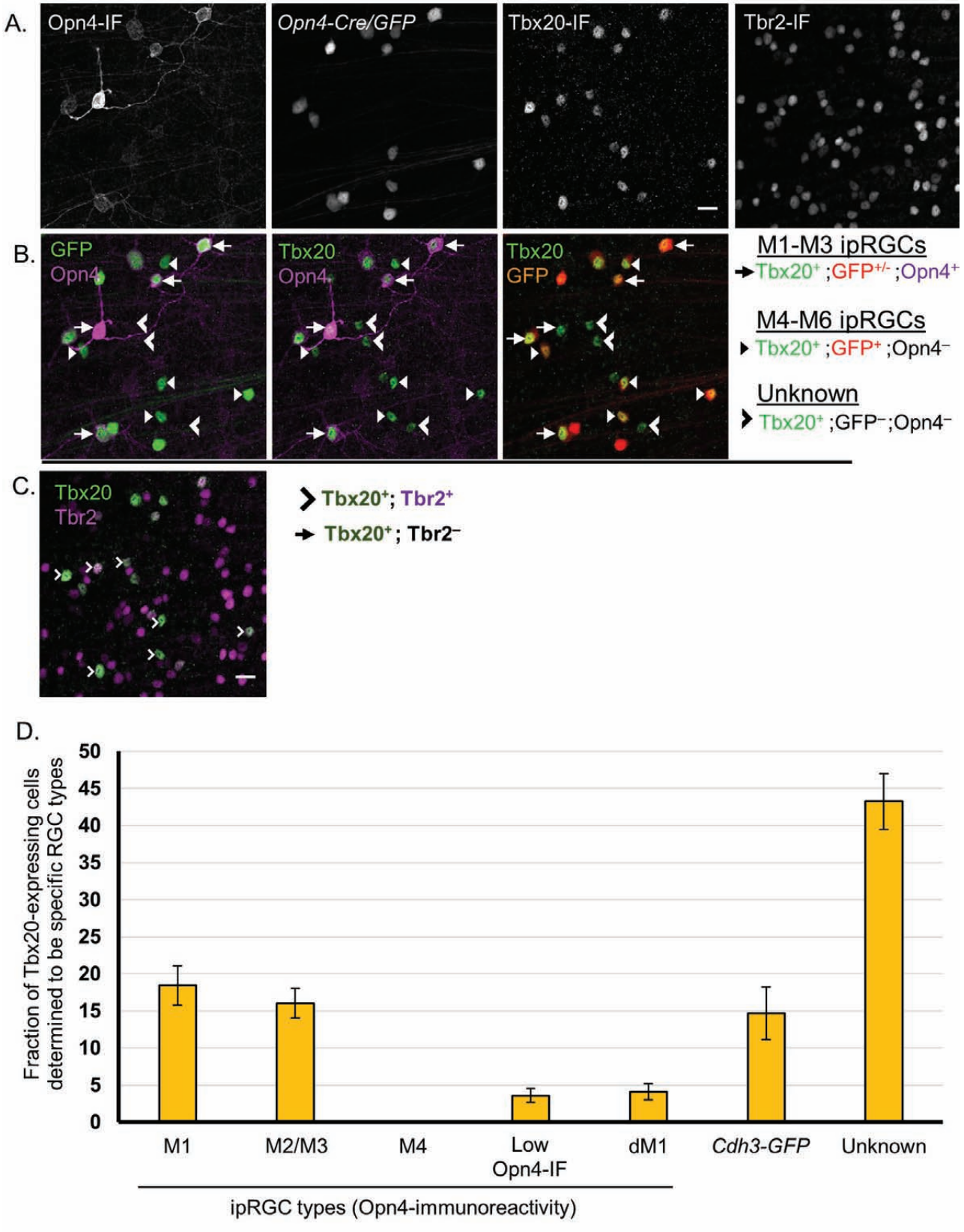

Figure 14.

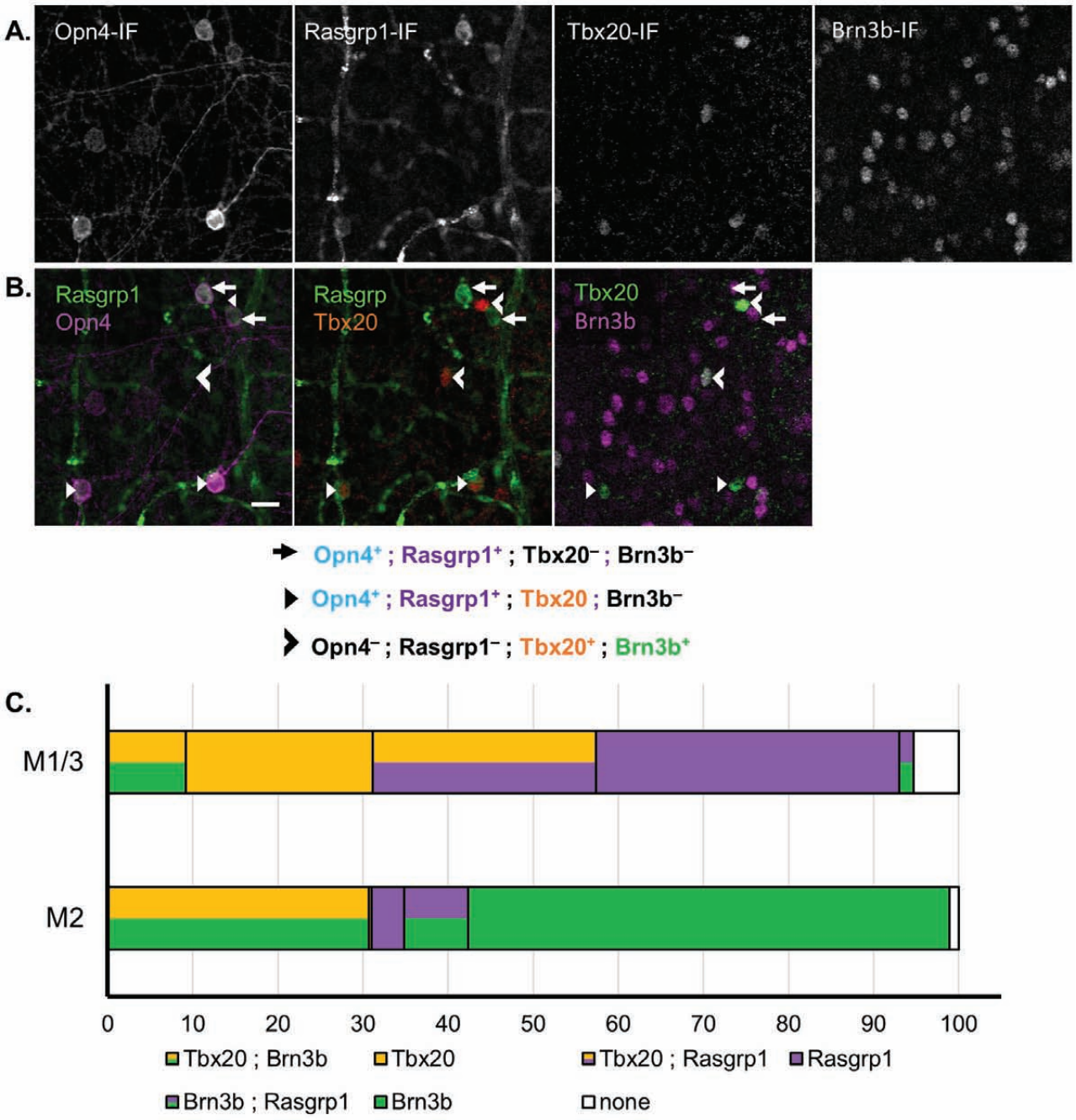

Figure 15.